

Chapter 3

TOWARDS A SOLUTION OF THE KNEE PROBLEM WITH HIGH ALTITUDE EXPERIMENTS

G. Di Sciascio and L. Saggese

INFN, sez. di Napoli and

Dipartimento di Scienze Fisiche dell'Università, Napoli, Italy

Abstract

The spectra of all Extensive Air Shower (EAS) observables can be described by power laws over a wide range of primary energies. In the PeV region the spectra show a small steepening, the so-called “knee”. This feature, known since more than 40 years, reflects the convolution of the steepening of all single mass spectra.

Despite large progresses in building new multi-component EAS experiments and in the analysis techniques to infer energy spectra and chemical composition, the key questions concerning the knee are still open. The main reason is that all the measurements in the knee region are only of indirect kind, i.e., are based on the reconstruction and interpretation of EAS observables.

One of the most important questions to be solved concerns the position of the proton knee. The knowledge of the primary proton spectrum is fundamental to understand the cosmic rays acceleration mechanisms and the propagation processes in the Galaxy.

A careful measurement of the proton spectrum in the energy region from 1 TeV to 100 PeV is one of the main tasks of future cosmic ray experiments. The need to measure showers with energy as low as 1 TeV to calibrate EAS data with the direct measurements imposes the construction of an unconventional air-shower array at high altitude. An experiment which can meet this requirement is the ARGONAT apparatus, located at the YangBaJing Cosmic Ray Laboratory (Tibet, 4300 m a.s.l.).

In this paper we review the present status of the knowledge in the cosmic ray studies around the knee. We discuss the capability of the ARGONAT experiment to discriminate between different models of the primary cosmic ray composition in the energy range $10 \div 500$ TeV, exploiting the digital response of the detector. The ability to select a high purity primary proton beam by operating a large area muon detector is also presented.

1. Introduction

Cosmic rays are the most outstanding example of accelerated particles. Understanding their origin and transport through the interstellar medium is a fundamental problem which has a major impact on models of the structure and nature of the universe. The primary cosmic ray energy spectrum extends up to about 10^{20} eV showing the following basic characteristics:

- a power-law behaviour $\sim E^{-2.7}$ until the so-called "knee", a small downwards bend around few PeV;
- a power-law behaviour $\sim E^{-3.1}$ beyond the knee, with a slight dip from $\sim 3 \cdot 10^{17}$ eV, sometimes referred to as the "second knee";
- a transition back to a power-law $\sim E^{-2.7}$ near $3 \cdot 10^{18}$ eV;
- uncertainty beyond 10^{19} eV, either a small cutoff or a continuation.

The energy range between 10^{14} and 10^{16} eV has long been recognized as crucial to understand the cosmic ray acceleration at all energies, because the knee appears to mark a transition from one acceleration process to another [1, 2]. Describing the processes by which galactic cosmic rays achieve their enormous energies remains a fundamental goal of astrophysics.

The most viable theory for the source of the bulk of cosmic rays is the shock acceleration of particles in SuperNova blast waves, which can provide the necessary energy input and naturally produce a power law energy spectrum with an index close to the value inferred from the observations. This SuperNova Remnant (SNR) acceleration mechanism is limited by the rate at which the particles can gain energy and by the lifetime of the shock. For a typical SNR, in the Lagage and Cesarsky [3] calculation this limit corresponds, for a particle of charge Z , to a total energy of $\sim Z \times 10^{14}$ eV, i.e., 10^{14} eV for protons and $\sim 3 \cdot 10^{15}$ eV for an iron nucleus. However, other versions of the model suggest that protons could be accelerated with little difficulty even up to $\sim 10^{15} \div 10^{16}$ eV. On the other hand, the knee could be attributed to propagation effects. In both cases, one would expect multiple bends due to the different elements bending at fixed rigidity with the consequence that the composition would become heavier above the knee.

A careful measurement of the single mass energy spectra in the knee region is of fundamental importance to discriminate between different interpretations. Due to the steep energy spectrum the direct measurement of the primary radiation can be performed, with adequate statistics, only for energies up to $\sim 10^{14}$ eV/nucleon.

The most recent results come from two balloon experiments, JACEE and RUNJOB [4, 5]. JACEE has measured the proton and Helium spectra up to ~ 800 TeV without observing any knee-like structure [6]. However, above 80 – 90 TeV the data does not have enough statistics to either assess or reject a presence of a break [7]. JACEE claims for a flatter He spectrum compared to the proton one, in agreement with the earlier SOKOL result [8]. The differential spectral indexes reported are $\gamma_p = (-2.80 \pm 0.04)$ and $\gamma_{He} = (-2.68 \pm 0.06)$.

The RUNJOB experiment in 1995 observed a PeV proton: this was the first event which confirmed by direct observation the existence of particles with energy per nucleon greater

than 10^{15} eV [9]. The data suggests, unlike JACEE, that the spectra of proton and helium nuclei are almost parallel, with slopes $\simeq -2.80$ for both, and an uncertainty between 10 and 20% [10]. From the beginning of this experiment, He flux is lower than that of most other experiments by about 40%. Even after the statistics is increased, this tendency is not changed [11]. JACEE data shows a gradual increase in the mass number at higher energies, while RUNJOB results seem to be almost constant over the wide energy range 20 – 1000 TeV/particle [12].

All the experimental evidences for a knee feature in the primary cosmic ray spectrum are of indirect kind, i.e., are based on the reconstruction and interpretation of EAS observables. Because of the reduced resolution in the measurement of the primary mass, the air shower arrays typically separate events as "proton-like" or "iron-like", with results which critically depend on MonteCarlo predictions. As a consequence, the results can be only displayed as a function of the total energy per particle with the so-called "all-particle" spectrum, i.e., as a function of the total energy per nucleus, and not per nucleon.

Despite large progresses in building new multi-component EAS experiments and in the analysis techniques to infer energy spectra and chemical composition, the key questions concerning the origin of the knee are still open. In particular, one of the most important questions to be solved concerns the position of the proton knee. In fact, the existing experimental data is in substantial disagreement: the proton spectrum measured by the TIBET-AS γ experiment shows a knee-like structure around 200 TeV, while the KASCADE data suggests a steepening at few PeV. Direct measurements carried out by RUNJOB and JACEE, as discussed above, do not exhibit any spectral break up to the highest measured energy (~ 800 TeV). The knowledge of the primary proton spectrum is fundamental to understand the cosmic rays acceleration mechanisms and the propagation processes in the Galaxy. A careful measurement of the proton spectrum in the energy region from 1 TeV to 100 PeV is one of the main tasks of the future cosmic ray experiments.

The problem of the knee, still not resolved after more than 40 years, can be traced back to the solution with an unconventional air shower array operated at high altitude (> 4000 m a.s.l.) able to separately sample the electromagnetic, muonic and hadronic components. At high altitude: (1) the shower fluctuations are reduced since the detector approaches the depth of the maximum longitudinal development; (2) the average shower size in the knee region is almost the same for both proton and iron primaries, providing a composition independent estimator of the energy; (3) the reduced attenuation in the atmospheric overburden allows one to observe EAS primaries with low energy (\sim TeV), thus approaching the direct measurements.

The ARGO-YBJ experiment, located at the YangBaJing (YBJ) Cosmic Ray Laboratory (Tibet, 4300 m a.s.l.), can provide a unique opportunity to study the cosmic rays in the knee region. In the actual set-up the detector, thanks to the low energy threshold and the high granularity sampling, can study the cosmic ray phenomena by (a) detecting the γ -ray emission from SNR in the energy range 0.2 – 20 TeV and (b) discriminating between the different models of the primary cosmic ray composition in the energy range $10 \div 500$ TeV.

In this paper we review the main experimental results of cosmic ray measurements in the knee region made with ground-earth based detectors and discuss the data analysis problems with particular attention to the open questions in the MonteCarlo code development. Then, we present the capability of the ARGO-YBJ experiment to discriminate between dif-

ferent models of the primary cosmic ray composition in the energy range $10 \div 500$ TeV, exploiting the digital response of the detector. The ability to select a high purity primary proton beam by providing the array with a large area muon detector is also discussed. Finally, suggestions about the opportunity of study the EAS cores at high-altitude by means of a hadron calorimeter are presented.

2. EAS Experiments

Cosmic rays are measured with a variety of techniques from different locations: in space, high in the atmosphere, at the Earth surface, underground. The location and the techniques depend on the intensity of the radiation and on the observables. Around the knee of the spectrum one expects about 1 particle/m²·day. As a consequence, to study the cosmic rays in the very high-energy region many detectors distributed over large areas are needed.

Modern air shower arrays are designed to measure simultaneously different quantities. An example of multi-component apparatus operating at mountain altitude is the EAS-TOP experiment (Campo Imperatore, 2000 m a.s.l., 810 g/cm² atmospheric depth, INFN Gran Sasso National Laboratories) [13], which has been operated until the year 2000 to detect:

- *electromagnetic (e. m.) component*, by means of 35 scintillator modules (10 m² each) distributed over an area of $\sim 10^5$ m²;
- *muonic component* ($E_\mu > 1$ GeV), by means of a 140 m² detector consisting of 9 active planes separated by 13 cm thick iron absorbers. Each plane is made of two layers of streamer tubes for the muon tracking and one layer of proportional tubes for hadron calorimetry. In addition, the effective muon sensitive area is increased by 10 m² scintillator detectors positioned below 13 e.m. modules, each shielded by 30 cm of iron;
- *hadronic component*, via the 140 m² muon tracking structure which operates as a calorimeter by means of the active layers made of tubes operating in “quasi-proportional” mode;
- *atmospheric Cherenkov light*, by means of 8 telescopes positioned at ~ 100 m one from the other. Each of them houses three mirrors, 90 cm diameter and 67 cm focal length. Two of them were seen by arrays of 7 photomultipliers for a full field of view of $5 \cdot 10^{-2}$ sr, for measurements of the total Cherenkov light signal, and a wide acceptance for operating in coincidence with the e.m. and muon detectors;
- *EAS radio emission*, via 3 antennas 15 m high, located on different sides of the array, at distances of 200 m, 400 m and 550 m from each other, operating in two wave bands: 350 – 500 kHz and 1.8 – 5 MHz.

Moreover, its location has been chosen to have the further possibility of running in coincidence with the muon detectors MACRO and LVD operating inside the deep underground Gran Sasso Laboratories. The sites are separated by $\Delta h = 1000$ m in altitude (corresponding to ~ 3000 m w.e., and $E_\mu > 1.4$ TeV). The relative zenith angle is $\langle \theta \rangle \sim 30^\circ$.

The main experimental EAS observables sampled at the detection level to reconstruct the properties of the primary cosmic ray at the knee energies are the following:

1) Charged particle component

This is the basic observable measured in all EAS experiments. The charged component is dominated by electrons and positrons and is usually sampled by an array of detectors distributed over a large area. The sensitive area is very small, $< 1\%$ of the instrumented area, therefore this poor sampling is the source of an additional instrumental fluctuation which adds to the intrinsic large fluctuations of the shower development. The majority of EAS arrays do not distinguish between the charged particles, so that $N_e \sim N_{ch}$. From the measurement of the charged particles it is possible to determine the shower core position and, via a Lateral Density Function (LDF), calculate the total number of electrons at the observation level (size of the shower N_{ch}), from which infer the energy of the primary particle. In addition, by measuring the shower temporal profile the direction of the incident particle can be reconstructed.

The LDF of charged particles is of phenomenological nature, determined via MC simulations for the particular experimental set-up. The most used LDF is adapted from the Nishimura-Kamata-Greisen (NKG) function [14, 15]

$$\rho_{ch}(r) = \frac{N_{ch}}{2\pi r_M^2} \frac{\Gamma(4.5 - s)}{\Gamma(s)\Gamma(4.5 - 2s)} \cdot \left(\frac{r}{r_M}\right)^{s-2} \cdot \left(1 + \frac{r}{r_M}\right)^{s-4.5} \quad (1)$$

being r the distance from the shower core. Here N_{ch} is the total number of charged particles, the parameter s describes the shape of the distribution and is related to the longitudinal development stage (age parameter). The Moliere radius r_M is the distance within which about 90% of the total EAS energy is contained ($r_M \sim 80$ m at the sea level, increasing with altitude). The normalization constant is expressed in terms of the Gamma Function Γ . We note that, from MC simulations, the charged particle lateral distribution in proton-induced showers results considerably flatter than in the photon-induced ones. Therefore the lateral containment parameter r_M must be smaller (typically by a factor of 2, see for example [16]).

2) Muonic component

The muons sampled by air shower arrays are typically in the GeV energy range. In fact, they are measured by shielded detectors (scintillators, streamer tubes, Geiger-Muller counters) in order to absorb the electromagnetic component that reduces the muons identification efficiency because of the punch-through of hard γ -rays or electrons. The most sophisticated detectors also exploit some tracking devices, to better identify the particles.

Since the muons do not multiply, but only slowly lose energy by ionization, the muon content of an EAS after the maximum attenuates much slower than the electromagnetic one. This flat shower longitudinal profile reduces the fluctuations in reconstructing the primary energy from the muon size. But the absence of multiplicative processes induced by muons implies that their number is lower than that of electrons (in a typical shower $N_\mu/N_e \sim 0.1$) with a much flatter lateral distribution. As a consequence, the muons are typically poorly sampled, i.e., the sampling fluctuations cancel the advantage of reduced showers profile fluctuations.

The LDF of muons can be described by a Greisen-like formula [17] with parameters depending on the particular experimental set-up. As an example, in the EAS-TOP experiment the data ($E_\mu > 1$ GeV) have been fitted by

$$\rho_\mu(r) = C \cdot N_\mu \cdot \left(\frac{1}{r_0}\right)^{1.25} \cdot r^{-0.75} \cdot \left(1 + \frac{r}{r_0}\right)^{-2.5} \quad (2)$$

with $r_0 = 400$ m [18]. To minimize the bias due to the extrapolation of the muon lateral density function to unobserved large distances from the shower core, some experiments represent the EAS muon content via the so-called “truncated muon number”

$$N_\mu^{tr} = 2\pi \cdot \int_{r_1}^{r_2} \rho_\mu(r) r dr \quad (3)$$

With an appropriate choice of r_1 and r_2 , N_μ^{tr} can be used as a mass independent energy estimator [19].

The muon component is the most sensitive observable, in combination with the size N_e , to discriminate mass groups. In fact, for a given observation level, N_e is smaller for heavy showers with respect to proton ones with the same energy, while N_μ is typically larger for heavy primaries.

Finally, since the muons are produced in hadron decays, they are almost absent in photon-induced showers. Hence, a muon content measurement allows one to improve the signal to background ratio in gamma-ray astronomy.

3) Hadronic component

The spectrum of EAS hadrons retains important information about the primary cosmic ray spectrum, which is dominated by the lightest component, i.e., the protons. In addition, the study of the EAS hadronic cores is a useful tool to investigate the interaction models. In fact, this observable is based on the energy retained by the incoming primary, and therefore on different features (total cross section and inelasticity) of the high-energy hadronic process. As will be discussed in the following, the hadron rate is an observable highly sensitive to the non-diffractive inelastic cross-section and provides important information about the dissipative mechanisms which occur in the nuclear interactions.

The hadronic component sampling has been performed at different atmospheric depths using various experimental techniques, like calorimeters, emulsions chambers and magnetic spectrometers. The most interesting information is:

- a) the measurement of the total energy content in the EAS core (i.e., the energy not transferred to the e.m. and muonic components as measured at large core distances) and its absorption characteristics;
- b) the measurement of the so-called “unaccompanied hadrons”;
- c) the detection of peculiar events as, for example, the multi-structured events correlated to large p_T secondaries produced in hadron interactions.

4) Underground muons

The EAS high energy muons originate essentially from the first interactions of the cosmic rays in the atmosphere, thus carrying information about the hadronic interactions and the nature of the primary. Nevertheless, the measurement limitations due to the fluctuations in the muon multiplicity or to the finite size of the detector make difficult the way back to the primary characteristics. The uncertainties in the reconstruction of the corresponding EAS energy can be reduced, in principle, if the measurement is correlated to a surface EAS array. The most interesting results come from the correlated EAS-TOP/MACRO experiments [20].

5) Cherenkov light

The EAS arrays observe the showers at a fixed atmospheric depth. The main tool for removing this limitation is provided by the detection of optical emission in atmosphere (fluorescence or Cherenkov light). Fluorescence light can be exploited at primary energies $> 10^{17}$ eV. At the knee energies Cherenkov light provides the information about the longitudinal development of the shower, related to the rate of energy released in the atmosphere and therefore to the primary composition.

Optical photons are little absorbed in the atmosphere, therefore the Cherenkov lateral distribution is much broader than that of charged particles. In addition, their density is much higher. As a consequence, it is possible to construct an array of Cherenkov telescopes to perform high sensitivity measurements, with smaller area and wider spacing than necessary for equivalent measurements of charged particles.

The amount of light received from each altitude of the shower by telescopes can be reconstructed via simple geometry calculations once that the shower axis direction and the core distance are known. The amount of Cherenkov light, strongly correlated with the electron shower size, can be used to estimate N_e as a function of atmospheric depth from which the position of the shower maximum X_{max} can be calculated. This method is essentially geometrical and is independent of MC simulations except for the reconstruction of the angular distribution of Cherenkov light around the shower axis.

The Cherenkov intensity is proportional to the primary energy, while the slope of the Cherenkov lateral distribution depends on the depth of the shower longitudinal maximum X_{max} and hence on the mass of the primary. Therefore, the study of cosmic ray composition can be made sampling the lateral distribution, i.e., the Cherenkov photon density as a function of the shower core distance.

The mean X_{max} for a given primary type increases logarithmically with energy at an elongation rate of about 80 g/cm^2 per decade, although this value depends on the hadronic model used in the calculation. The expected X_{max} value is similar for two primaries of different mass but with the same energy per nucleon.

The observations of atmospheric EAS-Cherenkov light allow:

- a measurement proportional to the total e.m. energy deposit of the shower above the observational level;
- a real “calorimetric” energy measurement, if the shower is completely absorbed;
- the geometrical reconstruction of the development of the e.m. cascade in the atmosphere, by means of the temporal or angular distribution of the light signal;

- a reduction of the primary energy threshold;
- a good angular information on the arrival direction of the primary particle. The arrival direction can be obtained by measuring the time of flight among different telescopes.

Combined with TeV muon underground observations such technique can provide:

- information complementary to the shower size N_e and to the number of high-energy muons relevant to the analysis of the primary composition and interactions;
- a reduction of the EAS primary energy threshold of operation, with the possibility of performing measurements at primary energies very close to the surface energies of the muons reaching the underground level ($E_0 \sim \text{few TeV}$), i.e., in an energy region where only primary protons can contribute to the TeV muon flux.

Therefore the atmospheric Cherenkov light associated with the TeV muons provide an interesting tool for calibrating the simulations and checking the cross section for pion production in the forward region at energies $E_\mu \sim E_0/A$ with a known primary beam.

3. Analysis Techniques

The reconstruction of the primary cosmic ray spectrum from air showers measurements is typically carried out by an array of detectors spread over an area of several thousands of square meters sampling the charged particle lateral density. The difficulty of EAS observations is in the interpretation of the data, i.e., in the deduction of the primary particle properties (energy, mass number and angle of incidence) from the quantities measured in the experiments.

The general scheme of analysis in an indirect measurement of cosmic rays is the following:

1. From the experimental data, via some phenomenological functions determined by MC simulations, the EAS observables of the particular detector (N_e , N_h , N_μ , X_{max} , lateral distribution ...) are reconstructed.
2. The distributions of such observables are compared with those extracted from a detailed simulation of the EAS development in the atmosphere in which is made use of a trial cosmic rays spectrum.
3. The input spectrum is changed in order to optimize the comparison between the reconstructed and calculated distributions of EAS observables.

In the last few years more sophisticated analysis techniques have been exploited to infer energy spectra and chemical composition (for a review see, for example, [21]). Nevertheless, because of the reduced resolution of the air shower arrays in the measurement of the primary mass, the determination of the primary composition depends critically on Monte-Carlo predictions and the so-called *all-particle* spectra are typically published. The most recent multi-component EAS experiments enable the simultaneous determination of several observables on an event-by-event basis. In this manner, in principle, the correlated uncertainty on energy and mass can be disentangled [21].

The connection between the nature of the primary particle and the actual experimental results requires a detailed understanding of particle interactions at very high energies and at very forward scattering angles. Since, as will be discussed in the next section, there is still no information available from accelerators on this domain, we are faced with an intrinsic ambiguity on the interpretation of cosmic ray data. The ambiguity is governed by our poor understanding of two basic elements: (a) the behaviour of the inelasticity K , i.e., the fraction of the primary energy carried away by the secondary particles; (b) the composition of the primary cosmic ray spectrum, i.e., the mass number A of the primary particles. This problem has been referred to as the "inelasticity- K -mass-number- A uncertainty", or KAU problem [22].

3.1. Hadronic Interactions and Cosmic Rays

To build a MC simulation of the EAS development in the atmosphere, the knowledge of particle production in high-energy hadronic interactions (cross sections, multiplicity, rapidity and p_T distributions, inelasticity of the multi-particle production) is required. In contrast to electromagnetic processes, we are still not able to calculate hadronic cross sections and multi-particle production from first principles. In addition to our limited understanding of QCD the main sources of uncertainties in the description of hadronic interactions are:

- incomplete knowledge of particle production at current collider energies (only part of the phase space is measured);
- extrapolation to energies well beyond the current experimental data.

Up to now, the highest energy has been reached at Fermilab's Tevatron Collider (CDF and D0 detectors) and corresponds to a ~ 2000 TeV proton collision with a stationary proton. Brookhaven's Relativistic Heavy Ion Collider (RHIC) provides energies of > 100 GeV per nucleon in nucleus-nucleus collisions. As an example, a N-N collision at RHIC is equivalent to a $\sim 5 \cdot 10^{14}$ eV cosmic ray N-air interaction [23]. The LHC Collider when in operation at CERN will extend this energy up to $\sim 10^{17}$ eV equivalent cosmic ray primary energy.

Although the future experiments will cover most of the EAS knee region energy, this is not true for the angular (or rapidity) range coverage. In fact, most detectors do not cover angles within one or two degrees off the beamline. In the upper plot of Fig.1 the multiplicity distributions of secondary particles in $p\bar{p}$ collisions (in the energy range $10^3 - 10^7$ GeV) is shown as a function of the rapidity [24]. Vertical bands show the angular acceptance of the two collider experiments with the largest rapidity range coverage. From the plot it results that most of the secondary particles are detected. However, as can be seen from the lower part of the Fig.1, where the energy distribution of the secondary particles is shown, only a small fraction of the primary energy is measured by these detectors. In addition this fraction decreases with the increasing of the primary energy. In the Tevatron Collider about 80% of the final-state energy flow is estimated to be missing, while for LHC this quantity will be 95% [23].

In the cosmic ray coordinate system the target nucleon is at rest, then the effect is even more evident. If a 2 PeV proton collides with an air nucleus and continues with half its initial energy, acquiring 200 MeV/c transverse momentum in the collision, it makes an

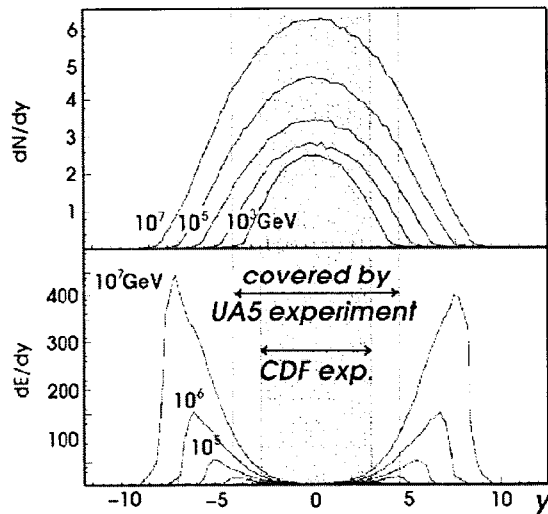


Figure 1. Particle (upper plot) and energy (lower plot) flow in $p\bar{p}$ interactions of different energies.

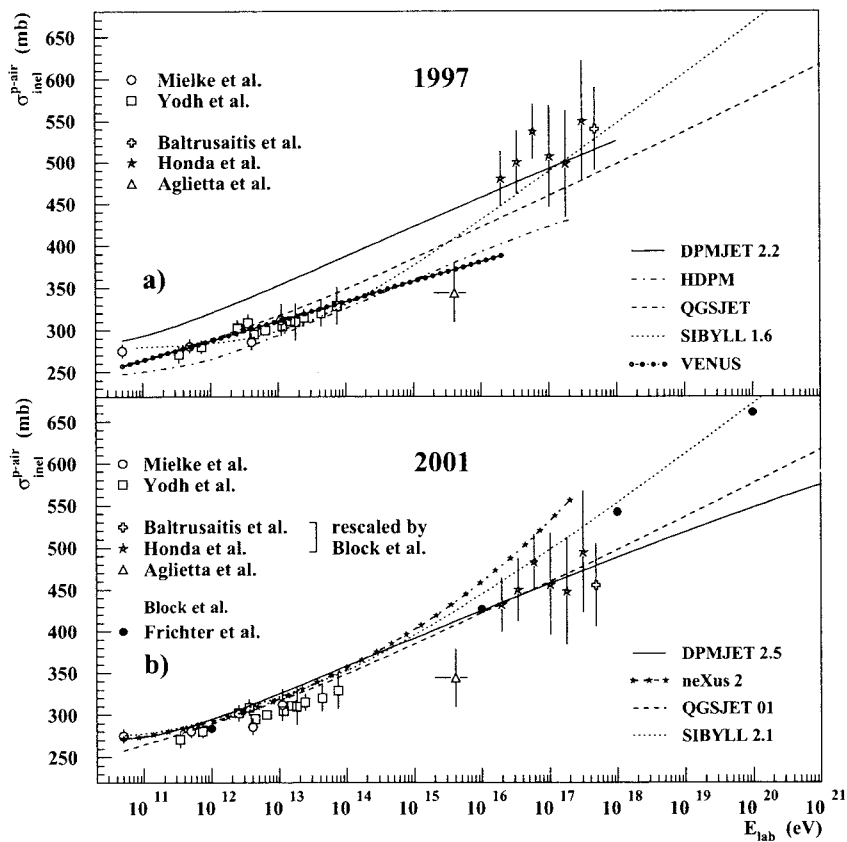


Figure 2. Inelastic p-air cross-sections from measurements and models [33]. *Upper panel:* Situation in 1997. *Lower panel:* Situation in 2001.

angle of only $0.2 \mu\text{rad}$ with its initial direction. The equivalent Tevatron process is a TeV proton colliding with a \bar{p} and scattering by an angle of about $0.4 \mu\text{rad}$, well within the cone that is unobserved by detectors [23]. Since the EAS development is dominated by this missing forward region, we lose the most important information for the simulation.

In addition, the extrapolations to higher energies are often based on inconsistent data. As an example, at $\sqrt{s} = 1.8 \text{ TeV}$ ($E_{lab} \sim 1.7 \text{ PeV}$) the measured $p\bar{p}$ cross sections are $72.8 \pm 3.1 \text{ mb}$ (E710 [25]), $80.03 \pm 2.24 \text{ mb}$ (CDF [26]) and $71.71 \pm 2.02 \text{ mb}$ (E811 [27]). The probability that these values are consistent with each other is only 1.6% [27]. The effect of a systematic uncertainty of about 5 – 10% on the EAS development can be relevant. In fact, an increase of $\sigma_{inel}(p\text{-air})$ by 10% implies a reduction of the high-energy ($> 100 \text{ GeV}$) hadrons number by up to 50% and of the electrons number ($> 3 \text{ MeV}$) by $\sim 15\%$ at sea level, in the case of 10^{14} eV vertical proton-induced showers [28].

As a consequence, one of the principal reasons for the large differences between the experiments is the degree of freedom in the various hadronic models. As an example, the reanalysis of the Haverah Park data, based on the CORSIKA code [29] with QGSJet [30] as the high energy interaction model, predicts a shower energy of $\sim 30\%$ smaller than the initial interpretation [31]. With this new energy determination all the highest-energy events from Haverah Park have an energy $< 10^{20} \text{ eV}$, and the estimated mass composition shifts towards heavier primaries.

Nevertheless, in the last few years large progress has been attained in EAS simulations. In fact, now most experiments use the same MC codes in order to reproduce the EAS development (CORSIKA code) and study the detector response (GEANT code [32]). In addition, the evolution of the models shows a clear convergence in their predictions up to 10^6 GeV .

The inelastic hadronic cross sections as well as the inelasticity of interactions are the main quantities which determine the elongation (slow aging) or the shortening (fast aging) of the EAS development. Lower cross section elongates, while higher ones shorten the longitudinal development. A highly inelastic interaction of a high-energy cosmic-ray proton could produce ground-level observables indistinguishable from those of a low inelasticity first interaction of a heavier primary nucleus with the same energy. In Fig.2 we show the inelastic p-air cross sections calculated in years 1997 and 2001, compared with some experimental data and theoretical models [33]. The cross section discrepancies between the models have reduced from 80 mb to about 20 mb in the few PeV region.

The inelasticity of hadronic interactions can be studied calculating the Feynman-x distribution x_F . The range $0.1 < x_F < 0.4$ corresponds to a moderate energy transfer to secondary particles, while in the diffractive region $x_F \geq 0.85$ the projectile loses only a small energy fraction and the largest portion is transported deeper in the atmosphere with the projectile remainder. Hence, the diffractive processes are the most important for the energy transport within an EAS. From the theoretical point of view there are some degrees of freedom in the diffractive description: the differences between the models exceed even by a factor of 3 [34].

A correct description of the diffractive phenomena, and of the inelastic cross-sections, is essential for the understanding of the observed hadron rates. A detailed study of muon and hadron rates has been carried out by the KASCADE Collaboration asking for triggers released by either high-energy hadrons ($E_h \geq 90 \text{ GeV}$) or a minimum number of 9 muons

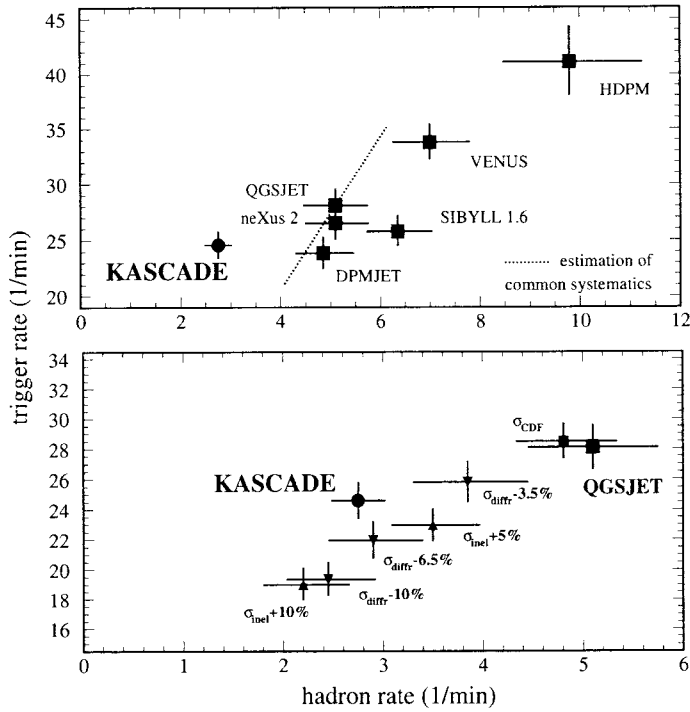


Figure 3. Trigger rate vs hadron rate in the KASCADE central detector. *Upper panel:* Data compared with different hadronic interaction models. *Lower panel:* Results obtained from the QGSJET model with modified inelastic cross section and diffraction dissociation.

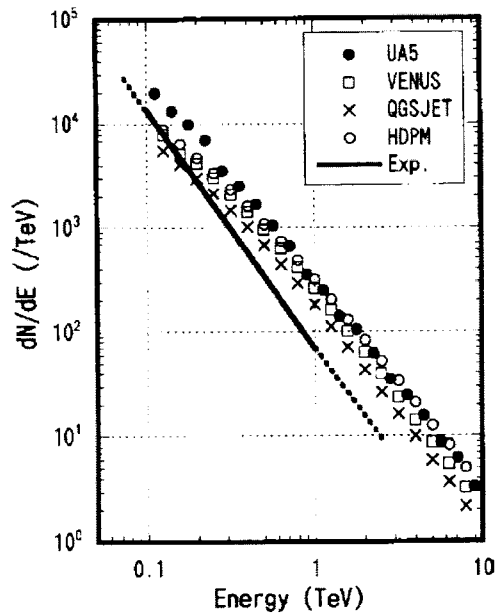


Figure 4. Differential energy spectrum of hadrons in EAS compared to some predictions by different simulations. The size range of the showers is $5 \cdot 10^6 \sim 10^7$.

($E_\mu \geq 0.50$ GeV) in the central detector. Such energy cuts applied to hadrons automatically select particles originating from the first high-energy interactions.

In the Fig.3 the trigger rate versus the hadron rate is plotted. As can be seen, none of the predictions agrees with the KASCADE results [28]: all models overestimate the hadron rate considerably, up to a factor of 3. Furthermore, there are also large discrepancies among the models. In order to study the sensitivity of the data to the details of the interaction models, several modifications have been applied to the QGSJet model. The results concerning their influence on the predicted trigger rates are shown in the lower panel of Fig.3. Increasing the inelastic p-air cross-sections by 5% (10%) reduces the predicted hadron rate by $\sim 27\%$ ($\sim 54\%$). Similar results arise from lowering the diffractive probability by up to 10% of the inelastic cross-section. Since the total inelastic cross-section is the better known quantity, is reasonable to presume that the uncertainty arises mostly from the diffractive processes. Hence, the KASCADE group attributed the overestimation of the hadron rate to an underestimate of the non-diffractive inelastic cross-section for nucleon-air collisions. In order to match data with hadronic models, the contribution of diffraction dissociation should be reduced by about 5 – 7% of the inelastic cross-section, i.e., to about half of the original contribution [34].

In Fig.4 the differential energy spectrum of hadrons measured at Mt. Chacaltaya (5200 m, 540 g/cm²) is compared with the expectations from simulations implemented with different models of hadronic interactions [35], for air showers of size $N_e = 5 \times 10^6 \sim 10^7$. The hadrons energy is in the range $0.1 \sim 1$ TeV. From the figure it results: (1) the energy spectrum of hadrons in EAS, predicted by the simulations, agree with one another both in the number and in the power index; (2) the data, instead, is not consistent with the simulation results in the number, while it is consistent in the power index. The number of hadrons by the experiment is smaller than those by the simulations, in agreement with the discussed results of the KASCADE experiment.

This tendency is consistent with the relationship between the families and the accompanied air showers reported by the same experiment [36]. That is, the number of high-energy γ -ray (≥ 2 TeV) in the family is smaller than that simulated. Therefore, at least either of the assumptions in the simulations, the energy distribution of produced particles or the primary composition, should be modified into the one of stronger energy subdivision. The following hypotheses are possible [35]:

1. The Feynman scaling law is violated in the forward region more strongly than assumed in the models.
2. The composition becomes heavier or the fraction of irons becomes larger than the one in low energy region to subdivide the energy between nucleons of heavy nuclei.

Here lies the source of the ambiguity, and from the knowledge available up to now, we have no clue for deciding in favor of one of these possibilities. This is the essence of the KAU problem [22].

4. Cosmic Ray Measurements

In Fig.5 a compilation of energy spectra obtained by various recent experiments is shown [37]. As can be seen, significant discrepancies exist among the different measurements concerning the position and the sharpness of the knee. It is still a matter of debate how much of these differences is due to experimental systematic errors and how much to uncertainties in the modelling of the shower development.

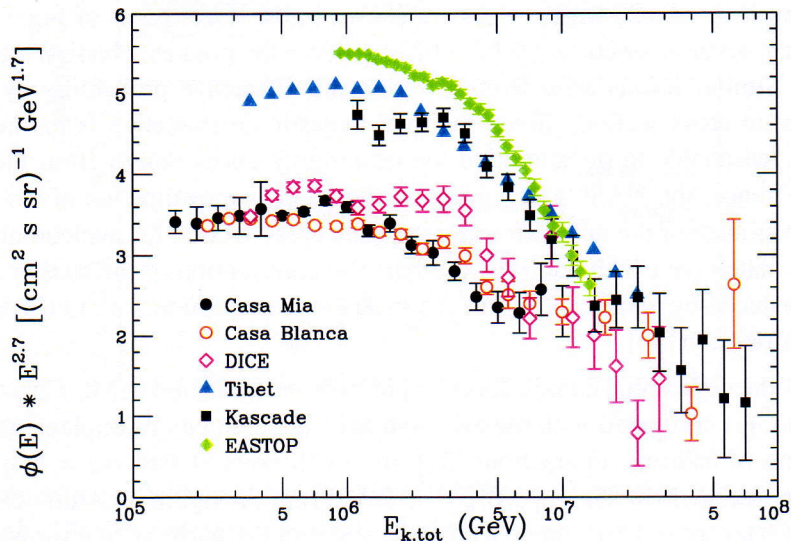


Figure 5. Recent measurements of the cosmic ray spectrum in the knee region.

The most recent results of EAS experiments will be summarized in the following (more comprehensive reviews can be found, for example, in [21, 34, 38, 39, 40]).

4.1. EAS-TOP Experiment

The multi-component EAS-TOP experiment has allowed the study of the primary cosmic ray spectrum by means of a lot of EAS observables.

In Fig.6 the differential shower size spectra at different zenith angles are shown. The knee is clearly visible and the corresponding size shifts towards lower values at increasing atmospheric depths, as expected for a knee at given primary energy. The attenuation length is $\Lambda_k = (222 \pm 3) g/cm^2$. The knee is observed at $N_e = 10^{6.1}$ in the vertical direction, $E_k = (2 - 4) \cdot 10^{15}$ eV. The knee is quite sharp, the change in slope occurring in a limited range of size ($\Delta \log(N_e) \sim 0.1$). The power indexes obtained for the energy spectrum are: $\gamma_1 = 2.76 \pm 0.03$ and $\gamma_2 = 3.19 \pm 0.06$ respectively below and above the knee [41].

The knee is also visible in the GeV muon size spectra, all zenith angles investigated (Fig.7). In this case the break is softened by the poissonian fluctuation of the number of detected muons. The knee, around $N_\mu^k \sim 10^{4.65}$, is independent of the number of detected muons, being visible at any core distance [42].

An interesting result comes from the relation between the electron and muon size slopes, which can be written as $N_\mu \propto N_e^\alpha$ with $\alpha \simeq 0.75$ in all angular bins: no change in the

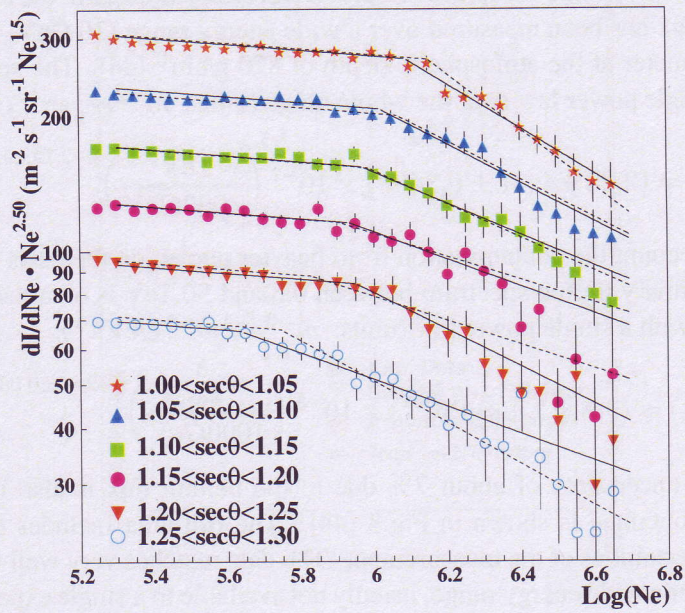


Figure 6. Differential shower size spectra measured by EAS-TOP at different zenith angles.

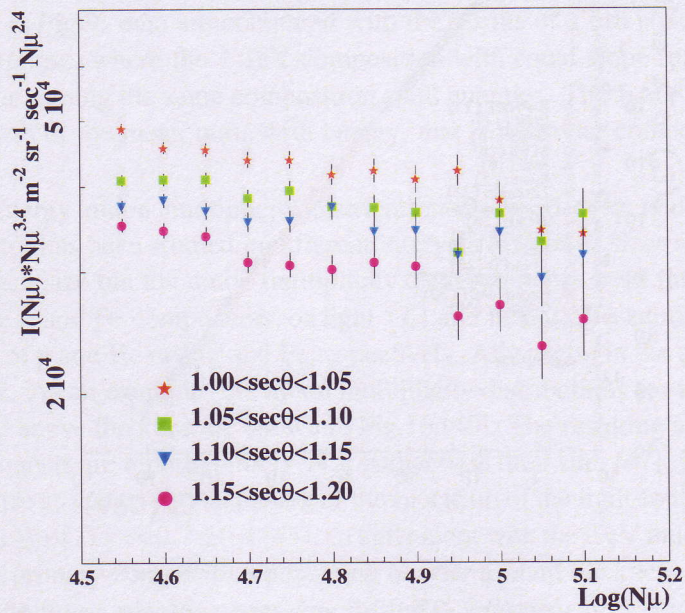


Figure 7. Differential muon size spectra measured by EAS-TOP at different zenith angles.

secondary production when crossing the knee region is seen, thus showing that, at least from this point of view, no new hadronic effects is necessary to explain the knee [43].

The hadron flux has been measured over a wide energy range (30 GeV – 30 TeV) with the hadron calorimeter at the atmospheric depth of 820 g/cm² [44]. The spectrum is well described by a single power law over the whole range (units: $m^{-2}s^{-1}sr^{-1}GeV^{-1}$):

$$S(E_h) = (2.25 \pm 0.21 \pm 0.34^{sys}) \times 10^{-7} \left(\frac{E_h}{1000GeV} \right)^{(-2.79 \pm 0.05)} \quad (4)$$

Taking into account the contamination from heavier nuclei, on the basis of direct measurements, the primary proton spectrum between 0.5 and 50 TeV is obtained and is found to be compatible with a single power law (units: $m^{-2}s^{-1}sr^{-1}GeV^{-1}$):

$$S(E_p) = (9.8 \pm 1.1 \pm 1.6^{sys}) \times 10^{-5} \left(\frac{E_p}{1000GeV} \right)^{(-2.80 \pm 0.06)} \quad (5)$$

A systematic uncertainty of about 7% due to the helium flux is also included. The proton spectrum obtained is shown in Fig.8 [44]. The full area includes the systematic and statistical uncertainties of the measurement. The data matches very well with the direct measurements over a wide energy range, usually not available to a single experiment, where they become statistically poor. The data show no evidence for a structure in the spectrum up to 100 TeV.

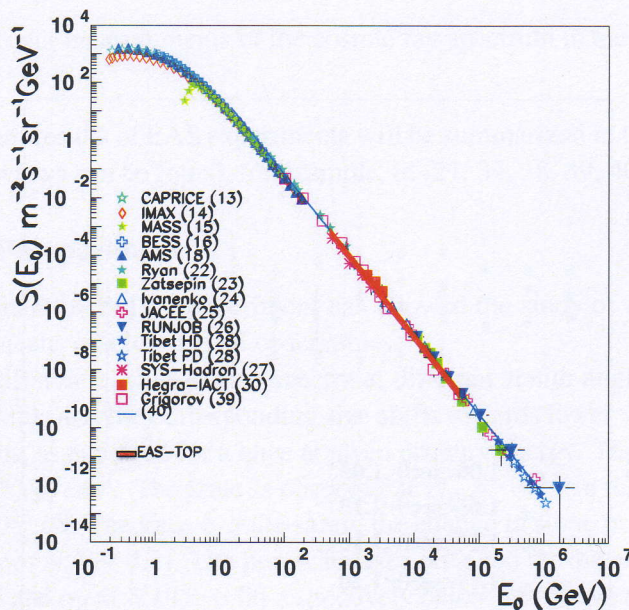


Figure 8. Primary proton spectrum. The full area represents the result of the EAS-TOP measurement and includes the systematic and statistical errors. Results from different experiments are shown for comparison.

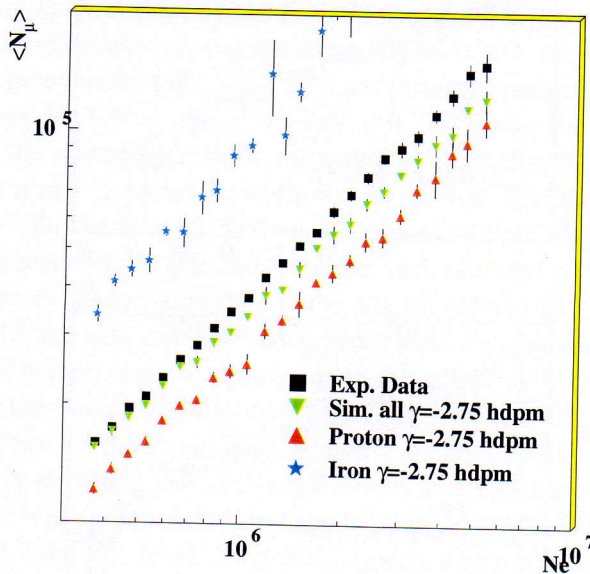


Figure 9. $\langle N_\mu \rangle$ vs N_e from EAS-TOP data (full squares) compared to a simulation with mixed composition (downward triangles), pure proton (upward triangles) and pure iron (stars) primaries.

The EAS-TOP collaboration studied the composition by analyzing the behaviour of $\langle N_\mu \rangle$ from vertical showers in narrow bins of N_e , corresponding to $\Delta N_e/N_e = 12\%$. The result is shown in Fig.9: data are compared with the results of a full simulation including the detector response, where the 1 TeV composition with equal slope for all components was used, thus assigning the same composition at all energies. The EAS-TOP data clearly suggests a growth of the mean mass with energy, that is a heavier composition above the knee [45].

The high energy muon multiplicity distribution observed deep underground by the MACRO detector has been studied in different intervals of shower sizes sampled by EAS-TOP. Within each size bin the muon multiplicity distribution has been fitted with a superposition of pure p and Fe components, or light (L) and heavy (H) admixtures containing equal fractions of p and He or Mg and Fe respectively. All spectra in the simulation have a slope $\gamma = 2.62$. As an example, the muon multiplicity distributions for two different size bins, below and above the knee are shown in Fig.10 [46]. The resulting energy spectra for p and Fe components are reported in Fig.11 together with their sum [47]. The data explains the observed knee as due to the steepening of the spectrum of the light component (p, He) at $E_k \sim 4 \times 10^{15}$ eV, of $\Delta\gamma = 0.7 \pm 0.4$ [48]. In agreement with the GeV muon data, this analysis points to a primary composition becoming heavier around the knee. The high energy muons used pertain to a rapidity region ($x_F > 0.1 \div 0.2$) which is different from the one explored with GeV muons (the central one): a good consistency of the CORSIKA/QGSJet model in describing the yield of secondaries in a wide rapidity region is thus obtained.

The proton, helium and CNO fluxes in the 20 \div 300 TeV energy range have been studied

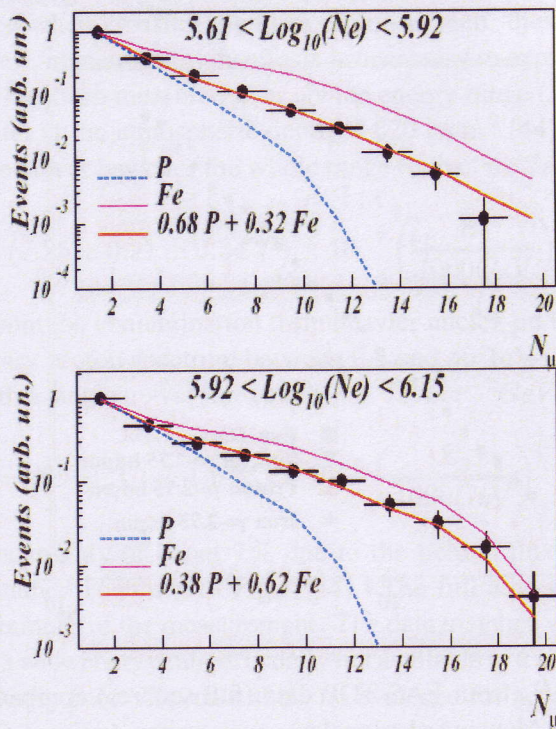


Figure 10. Muon multiplicity distribution measured with the MACRO detector in two size bins across the knee observed in the e.m. size sampled by EAS-TOP, compared with the results of the QGSJet model.

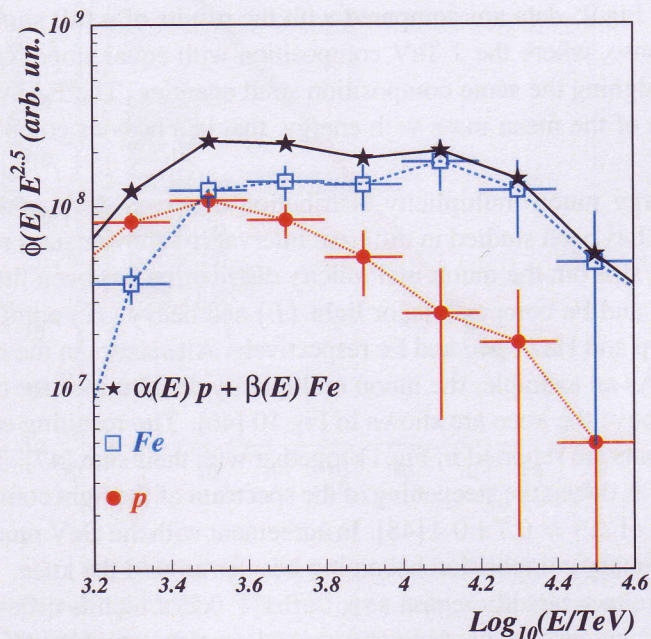


Figure 11. Energy spectra for p and Fe components, and their sum.

through the simultaneous detections of the high energy muons and the lateral distribution of Cherenkov light (C.l.) in EAS by the EAS-TOP and MACRO detectors. The EAS are selected via the muons detected deep underground by MACRO. Due to the shower selection through the high energy muon ($E_\mu > 1.3$ TeV, i.e. primary energy $E_o > 1.3$ TeV/nucleon), in the energy range $10 \text{ TeV} < E_o < 40 \text{ TeV}$ (10 TeV being the Cherenkov telescopes threshold energy) the selected primaries are mainly protons, for $40 \text{ TeV} < E_o < 100 \text{ TeV}$ they include both p and α particles, while for $E_o > 100 \text{ TeV}$ the CNO also contribute [49]. The “p+He” flux at $E = 80 \text{ TeV}$ and the “p+He+CNO” one at $E = 250 \text{ TeV}$ are thus obtained. Frequencies are selected from the rates obtained by introducing inside the simulation the primary spectra according to the JACEE [6] and RUNJOB [9] data. As can be seen from Fig.12, the data matches very well with the simulated points according to the JACEE proton and helium spectra, showing both the adequacy of the CORSIKA/QGSJet code in describing the cascades in this energy range and of the JACEE flux in the $20 \div 120 \text{ TeV}$ region. The error on the x axis represents the uncertainty on the EAS core position, while on the y axis statistical and systematic errors are summed up in quadrature. The agreement is worse when frequencies are calculated using the RUNJOB data (Fig.13), the difference being at 2 the s.d. level. The data supports a helium spectrum harder than the proton one, $\gamma_p \sim 2.8$ vs. $\gamma_{He} \sim 2.6 - 2.7 \sim \gamma_{CNO,Fe}$, with the preponderance of the helium primaries around the knee. In fact the ratio $\frac{J_p}{J_{p+He}}(80 \text{ TeV}) = 0.29 \pm 0.09$ implies that around 100 TeV the helium flux dominates over the proton one. By subtracting the measured proton flux the ratios of p, He and CNO components at 250 TeV can be expressed as: $J_p : J_{He} : J_{CNO} = (0.20 \pm 0.08) : (0.58 \pm 0.19) : (0.22 \pm 0.17)$ [50].

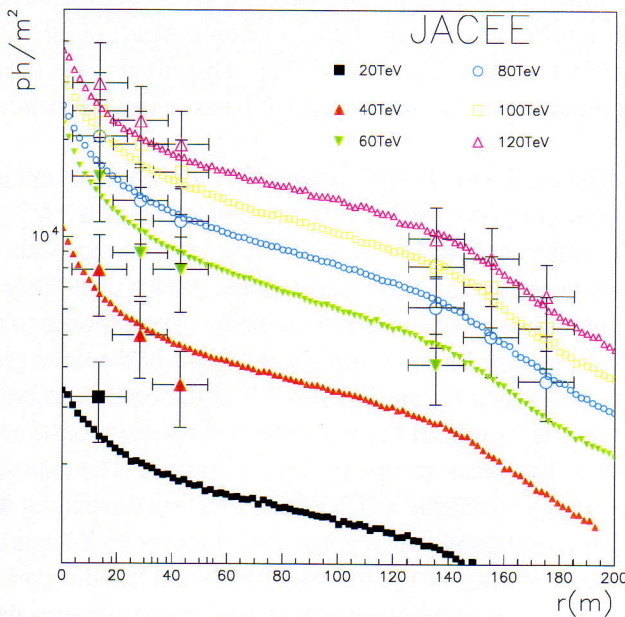


Figure 12. Measured Cherenkov light lateral distributions compared with simulated ones ($290 < \lambda < 630 \text{ nm}$) using the JACEE spectra.

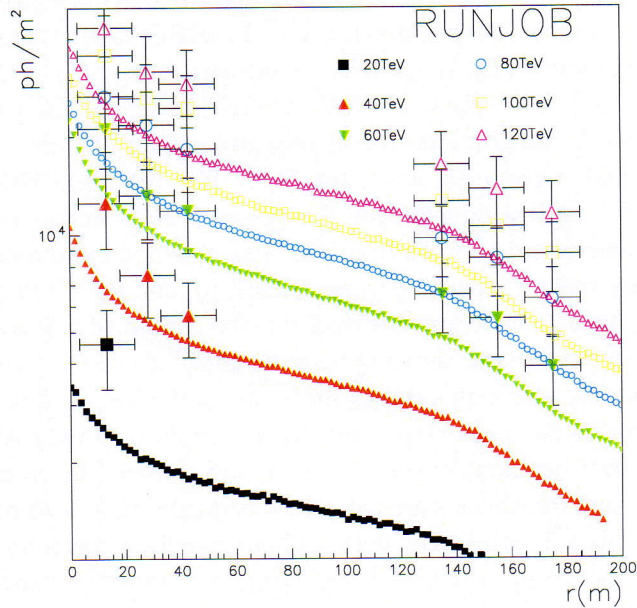


Figure 13. Same as Fig.12 but using the RUNJOB spectra.

4.2. KASCADE Experiment

The KASCADE experiment consists of a multi-detector set-up addressed to measure simultaneously the electromagnetic, muonic and hadronic components of air showers, providing a large set of observables for each single event [51]. This allows one to infer the primary mass and energy of primaries on an event-by-event basis using sophisticated multivariate analysis methods [21].

The main observables are the total electron size N_e , the number of muons in the 40 - 200 m range from the shower core (the so-called “truncated muon size” N_{μ}^{tr}), the local muon densities measured for different thresholds, the number and energy sum of reconstructed hadrons. The frequency spectra of all these observables show a clear knee-like structure at same integral event rates. Since a same intensity of the flux corresponds to an equal primary energy, this result is a strong hint for an astrophysical origin of the knee phenomenon.

The basic analysis performed by the KASCADE collaboration in order to extract the primary energy and mass is to unfold the two-dimensional electron-muon size spectrum into the energy spectra of five mass groups (p, He, C, Si, Fe). The size spectra are in fact the convolution of the energy spectrum with a kernel function describing the probability of a given primary to produce a shower with a given size. This method leads to the all-particle energy spectrum as a superposition of the spectra of light and heavier particles.

In Fig.14 the results of the unfolding method are shown for two different hadronic interaction models (QGSJet and SIBYLL) embedded in the CORSIKA code [52, 53].

Despite large differences in the relative abundances of the mass groups, the all-particle energy spectrum is similar for both models. In both calculations the knee at about 5-6 PeV

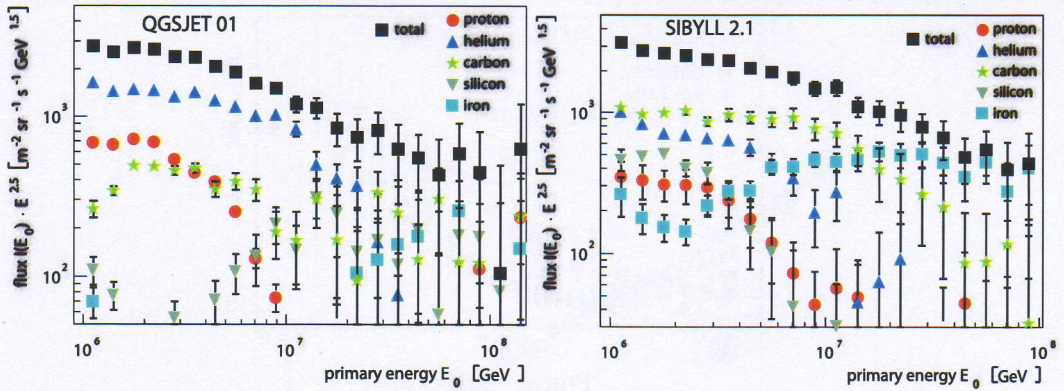


Figure 14. Cosmic ray spectra reconstructed by means of the KASCADE unfolding procedure. Left side: analysis based on the QGSJet hadronic model; right side: based on the SYBILL one.

is due to the decreasing flux of light primaries. For the light particle (proton and helium) spectra a knee-like structure is clearly visible. In the carbon spectrum there is only a small hint for a knee around $\log(E) \sim 7.3$, while for the heavier particle ($A > 20$) component a knee is missing between 1 and 10 PeV, thus suggesting an increase of the mass above the knee. The results using different unfolding methods show the same behaviour.

The ratio $Y = \log N_{\mu}^{\text{tr}} / \log N_e$ provides an interesting parameter to estimate the primary mass, which is found to be gaussian distributed at fixed A [54]. An example is presented in Fig.15. Clearly, a superposition of different particle types (represented by the lines) is required to account for the experimental distribution. It is noteworthy that its left and right are nicely described by the proton and iron simulations, respectively. Performing such an analysis for different bins of shower sizes yields confirm of an increasingly heavier composition for energies above the knee.

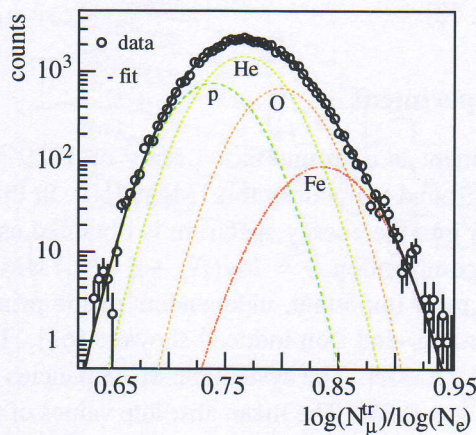


Figure 15. Event-by-event distribution of the muon/electron ratio measured by KASCADE for a primary energy of $E \simeq 3 \cdot 10^{15}$ eV. The lines show the results of CORSIKA/QGSJet model.

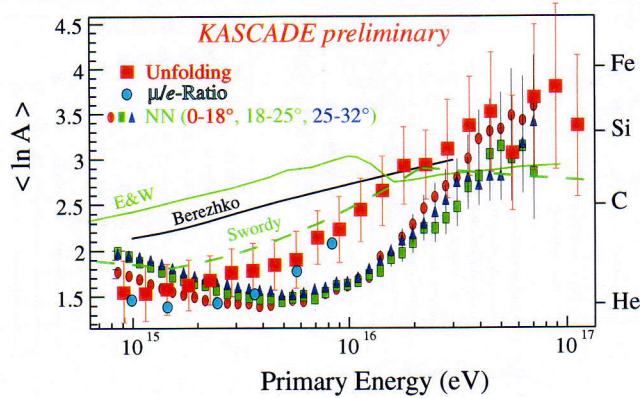


Figure 16. Mean logarithmic mass as a function of the primary energy. The KASCADE data (symbols) refers to different analysis.

The KASCADE data suggests that the light component is responsible for the knee $E_k^p \sim 4 \cdot 10^{15}$ eV, while for the iron nuclei a rigidity cut-off at $E_k^{Fe} \sim 26 \cdot E_k^p$ is possible [55].

The mean logarithmic primary mass $\langle \ln A \rangle$ as a function of the primary energy is reported in Fig.16. The data are compared to theoretical calculations made by [56, 57, 58] and to other experimental results from KASCADE [59]. In the energy range from about 1 PeV to 4 PeV the composition shows a weak decrease in the mean logarithmic mass by about 0.5 units. Similar trends have been observed also by Cherenkov air shower measurements (see the discussion on BLANCA and DICE results in section 4.5).

By comparing different methods and sets of EAS observables, systematics can be reduced and the hadronic interaction models underlying the different analysis of energy and composition checked. The SIBYLL and QGSJet models are able to describe the data at lower and at higher energies, respectively, but none of these gives a satisfactory description of the whole data set in a way consistent to obtain a final result on chemical composition and energy spectrum [34, 53].

4.3. CASA-MIA Experiment

The CASA-MIA experiment is a ground-based array of 1089 surface particle detectors (CASA) and 1024 underground muon detectors (MIA) [60]. In this experiment the conversion of the size spectrum into the energy spectrum is obtained using the muon size information. In fact, the size combination $\psi = \log(N_e + \xi \cdot N_\mu)$ was found to be linear vs the primary energy E_0 and, most important, independent of the primary mass. This relation is shown in Fig.17 for proton- and iron-induced showers [61]. The code used in the calculation is the CORSIKA/QGSJet. The systematic discrepancies in energy assignment for different primary masses are $< 5\%$. The mean absolute values of the energy reconstruction errors vary from $\sim 25\%$ at 10^{14} eV to $\sim 16\%$ for $E_0 \geq 10^{15}$ eV.

The energy spectrum thus derived is shown in Fig.18. As expected, the knee is located at the same primary energy for any atmospheric depth. The change in the spectral index does not appear to be sharp, but rather to undergo a transition over the range of energies $10^{15} - 10^{15.4}$ eV. The electron size spectrum, on the other hand, shows a sharper change

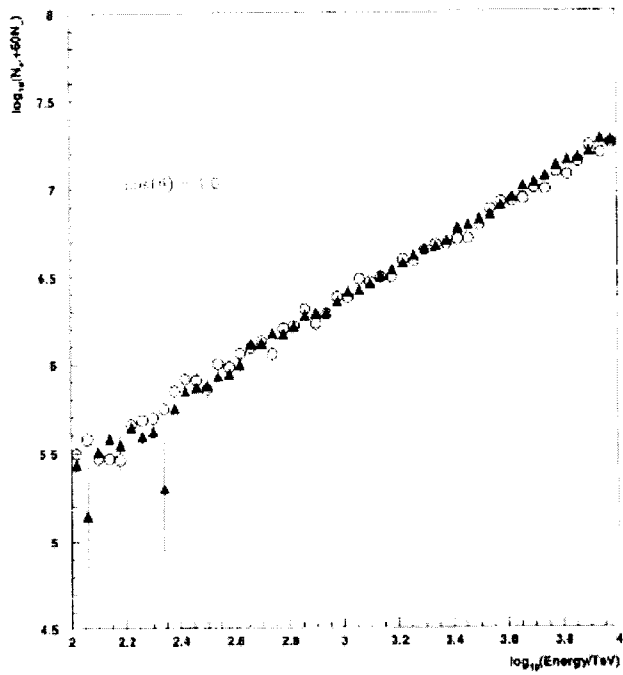


Figure 17. $\log(N_e + \xi N_\mu)$ versus energy for simulated proton (open circles) and iron (full triangles) primaries.

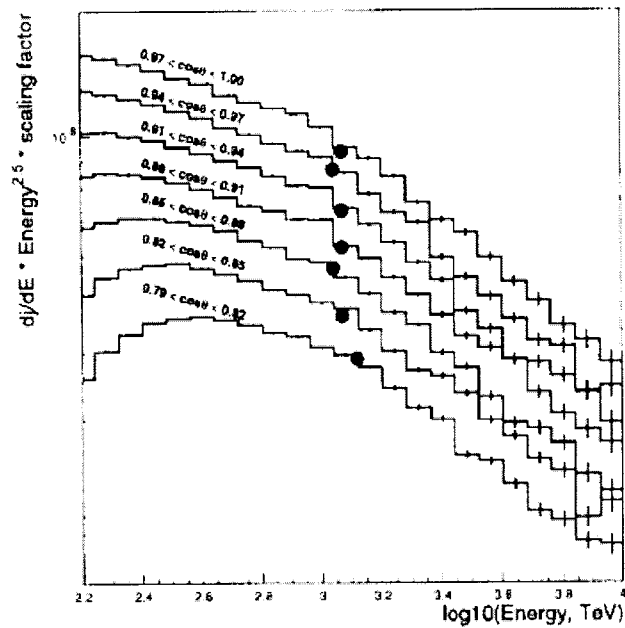


Figure 18. Primary energy spectrum from CASA-MIA data.

[61].

With this composition independent all-particle spectrum, the question of the sharpness of the knee of the cosmic ray energy spectrum has been investigated by the CASA-MIA collaboration. The data favours a change from light to heavy composition over the knee energy region. If the knee is a result of cosmic rays escaping the galaxy or is due to the upper limit of SuperNova acceleration processes (proportional to the charge Z), then we expect that the lighter nuclei exhibit the knee at lower energies with respect to the heavy ones. Since at the observation level the heavier cosmic rays show smaller sizes than their equal energy but lower mass counterparts, it is possible, in principle, that different spectral breaks from several nuclear species are more close in measured size, showing a much sharper knee in the size spectrum with respect that observed in the energy spectrum. As a consequence, the sharpness of the size spectrum break observed by CASA-MIA is evidence that the similar sharpness observed in other experiments, which derived the energy spectrum only using the shower size, could have originated by a compositional change in the knee region [61].

The primary composition is studied by CASA-MIA using three parameters: the density of surface particles, the slope of the lateral distribution near the core, and the density of muons at large core distances. An experimental event is assigned to the "light primary" or "heavy primary" class depending on the distance from the proton or iron simulated showers in the plane of the adopted variables. In order to quantify the decision a discriminant analysis based on the "K Nearest Neighbour" (KNN) test was exploited [62].

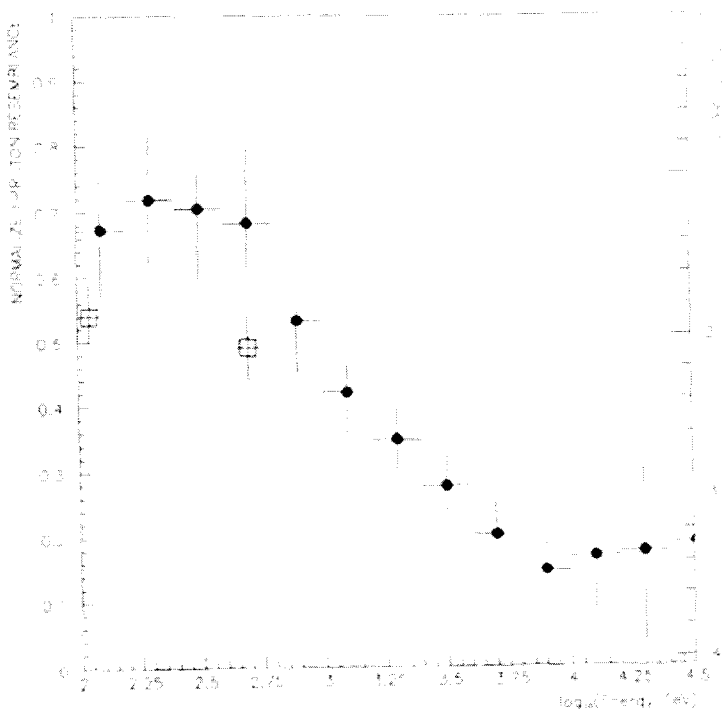


Figure 19. Normalized proton resemblance plot. The open squares give the estimated results for a JACEE-like composition.

The "proton resemblance", defined as the average fraction of K nearest neighbours

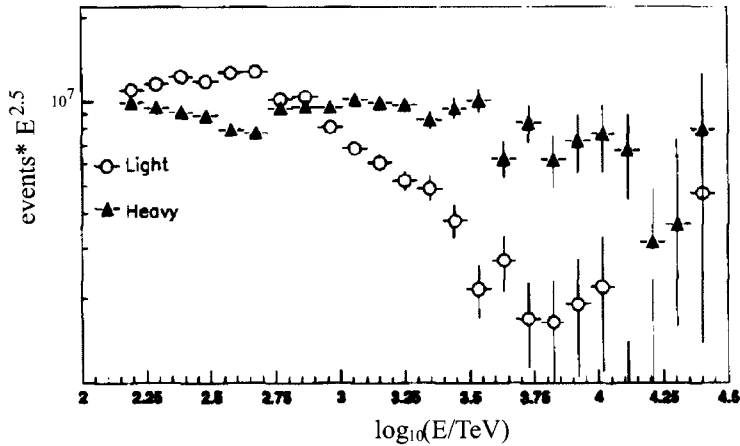


Figure 20. CASA-MIA events selected by the KNN tests as "light" or "heavy", binned following the reconstructed energy.

which are protons, is shown in Fig.19 for $K = 5$, normalized such that a pure proton composition would lay along the top of the plot and a pure iron along the bottom border. The trend towards a heavier composition above the knee is evident.

The energy spectra from CASA-MIA data are plotted in Fig.20 separated in two composition groups: "light", with more than half proton nearest neighbors and "heavy", with less than half. The spectra appear similar below 500 TeV, where the lighter component spectrum steepens. The heavier component does not show such a knee-like feature at that energy; the estimated spectral change is at about 10 times the energy corresponding to lighter component knee [62]. The spectra are consistent with the idea of cutoffs proportional to the particle rigidities.

4.4. TIBET-AS γ Experiment

The TIBET-AS γ experiment is a hybrid detector consisting of an EAS array operating at high altitude (Yangbajing, Tibet, 4300 m a.s.l., 606 g/cm²) in correlation with an emulsion chamber and a burst detector array. The emulsion chambers and the burst detectors are exploited to detect high-energy air shower cores accompanying by EAS induced by cosmic rays with energies above 10¹⁴ eV. The shower size measurable by each burst detector ranges from 10⁴ to 3·10⁶ particles, roughly corresponding to sub-showers with energies ranging from several times 100 GeV to about 300 TeV.

The high altitude is particularly suitable for the measurements in the knee region since: (1) air showers induced by primaries with energies in the range $\sim 10^{15} - 10^{17}$ eV reach their maximum development roughly in the 500 - 600 g/cm² atmospheric depth interval, thus their size fluctuations are at minimum; (2) in this energy range the average shower size is almost the same for both proton and iron primaries. These facts enable us to estimate the primary energy with a reduced ambiguity by measuring only their shower size, almost independently of the cosmic ray composition.

The overall primary energy spectrum shows a gradual steepening of the slope at energies between 10^{14.75} and 10^{15.85} eV, around 10^{15.25} eV [63]. This smooth shape of the

energy spectrum in the knee region is similar to that found by the CASA-MIA experiment. By means of a modest energy shift (20%, about the statistical uncertainty in energy assignment due to shower fluctuations) the two independent TIBET-AS γ and CASA-MIA spectra agree quite well [61]. Both experiments have obtained the all-particle energy spectrum in a way almost independent of the primary composition (only the size N_e at high altitude and the linear combination of electronic and muonic sizes in CASA-MIA experiment at a lower altitude). This result suggests that a method of examining the spectrum sensitive to the primary mass reproduces a sharp break, while a smooth knee is obtained when a composition insensitive technique is exploited. As a consequence, composition factors, or detector effects, may play a relevant and neglected role in several measurements.

In Fig.21 is shown the energy spectrum of primary protons reconstructed using data obtained with the burst detectors and the air shower arrays and applying a neural network analysis [65, 66].

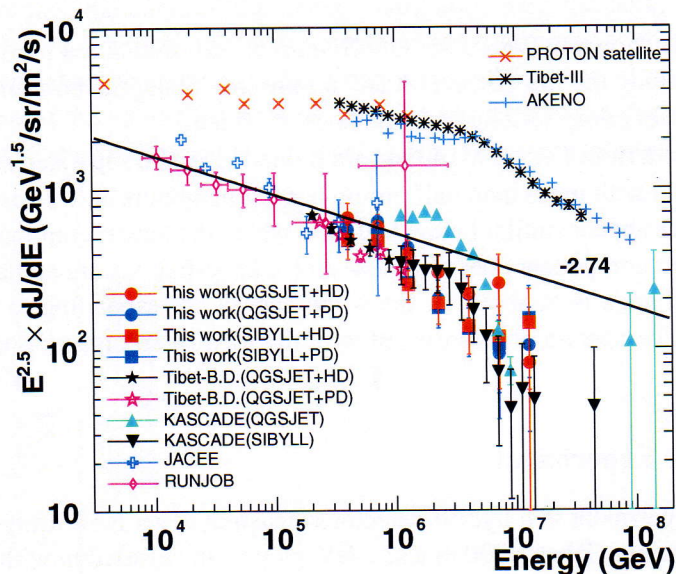


Figure 21. The proton spectrum obtained by the TIBET-AS γ hybrid experiment compared with results from other experiments.

The spectral index above the knee is about -3, steeper than that obtained by direct measurements at lower energies, suggesting that the proton spectrum should steepen around 200 TeV. Assuming that all single masses have their break point proportional to their atomic number, the main component responsible of the knee structure in the all-particle spectrum is the nuclei heavier than helium component [64, 65, 66].

In addition, the comparison with the KASCADE experiment [67] shows that their results strongly depend on the interaction models (Fig.22), probably because the low-energy muons may not be a suitable parameter for separating the air showers into different primary mass groups [66].

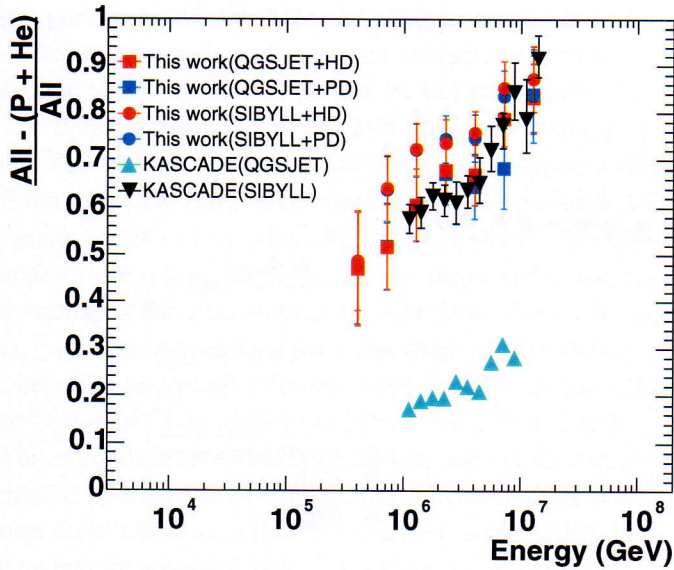


Figure 22. Fraction of the primary cosmic rays heavier than helium nuclei. The Tibet results are compared with those by KASCADE experiment.

4.5. The BLANCA and DICE Cherenkov Detectors

The BLANCA and DICE Cherenkov detectors has both operated at the same site of the CASA-MIA experiment for which it provides the shower core position and the arrival direction.

The BLANCA detector [68] consists of 144 angle-integrating Cherenkov light telescopes which measure the lateral distribution of the Cherenkov photons. BLANCA uses the CASA-MIA trigger which imposes an energy threshold of about 100 TeV on the Cherenkov array. For each event, the data is converted to photon densities, producing a Cherenkov lateral distribution which is fitted with an empirical function. This function is exponential in the 30 - 120 m range from the shower core while for larger distances is a power law with three parameters: a normalization factor C_{120} (i.e., the Cherenkov intensity 120 m from the core), an exponential slope s and a power law index β . The energy of each EAS is derived using only the C_{120} and s parameters. The BLANCA energy resolution for a single air shower is about 12% for a 200 TeV shower, improving to $\sim 8\%$ for energies above 5 PeV.

The differential all-particle cosmic ray spectrum measured by CASA-BLANCA is shown in Fig.23, compared with the results reported by other experiments [68]. The different results are consistent given the 20% or more energy systematic error typical of air shower measurements. As can be seen from the figure, the CASA-BLANCA data shows a smooth change rather than a sharp break of the spectrum. The knee region is near 3 PeV with a width of ~ 0.5 decades in primary energy.

The CASA-BLANCA measurement of X_{max} is shown in Fig.24, compared with other results up to the Fly's Eye energies [68]. The "direct" point shows the X_{max} value expected based on balloon direct measurements.

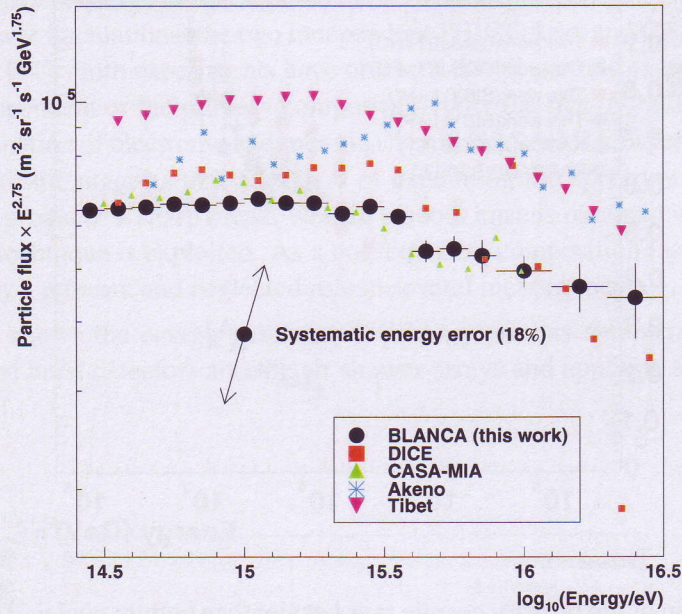


Figure 23. The differential all-particle cosmic ray spectrum measured by CASA-BLANCA, compared with other experiments. The diagonal bar shows the effect of a possible systematic energy shift of $\pm 18\%$.

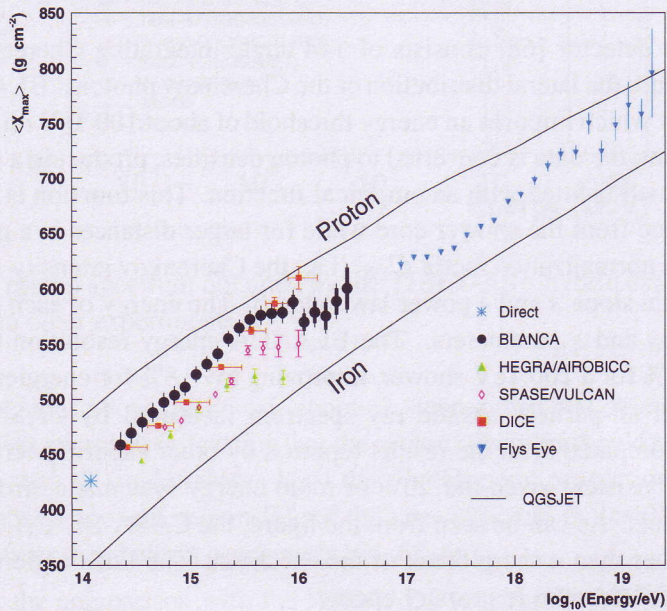


Figure 24. The CASA-BLANCA measurement of X_{max} compared with other results.

The data is consistent with a mixed composition which is lighter approaching the knee and heavier at higher energies. Furthermore, at low energies the results are consistent with those expected from direct measurements and at high energies with the Fly's Eye data. A multi-component fit with four masses (p, He, N, Fe) suggests the same composition trends exhibited by the mean quantities, i.e., an initially mixed composition that results lighter between 1 and 3 PeV and then becomes heavier with increasing energies.

The DICE detector [69] consists of 2 imaging telescopes each with a 2 m diameter and a focal plane made by 256 close packed photomultipliers. The Cherenkov light size and the shower maximum development X_{max} are the measured quantities. The Cherenkov size is obtained by summing the total amount of light detected by each phototube cluster. The location of X_{max} is determined by fitting the shape of the shower image in each photomultiplier cluster. An important difference between DICE and other detectors which fit the lateral distribution of Cherenkov light is that this estimate of X_{max} is based on simple geometry and does not depend on MC simulations, except for calculations necessary to determine the angular distribution of Cherenkov light around the shower axis. The primary energy spectrum from DICE events in coincidence with CASA-MIA is shown in Fig.23. The knee is at an energy around 3 PeV. The values measured for X_{max} are shown in Fig.24 as a function of energy. The various experiments show a fair agreement, although the DICE data suggests a lighter composition at higher energies.

5. Theoretical Models for the Knee

As discussed in the previous sections, due to the contradictory experimental results, the reason for the steepening of the primary cosmic ray spectrum in the PeV region is still unclear. The theories addressed to explain the origin of the knee are essentially of four types [21, 52, 70, 71]:

- 1) *Acceleration*: there is a general agreement in believing that the bulk of cosmic rays are produced in SuperNova Remnants. In fact, they can provide the power ($L_{CR} \sim 5 \cdot 10^{40}$ erg/s) required to justify the observed energy density of cosmic rays (≈ 1 eV/cm³). Charged particles in the interstellar medium surrounding the pre-SuperNova star may get trapped in the highly supersonic shock wave generated by the SN explosion. Repeated reflections on both sides of the shock front lead to an acceleration via the so-called "first order Fermi mechanism", which naturally produces a power law energy spectrum with differential index ~ 2 at the source.

This acceleration process appears to have an upper limit which depends on the rate at which the particles can gain energy and on the shock lifetime. Simple dimensional estimates show that the maximum energy in a SNR is limited to $E_{max} \sim Z \times (R_{SNR} \times B)$, where Z is the charge of the cosmic ray isotope and R_{SNR} , B are the size and the magnetic field strength of the acceleration region. In the classical analysis performed by Lagage and Cesarsky [3] this limit corresponds to about $Z \times 10^{14}$ eV. A more recent examination of the astrophysical parameters suggests an upper limit in acceleration of $E_{max} \approx Z \times 10^{15}$ eV [57, 72]. In a model proposed by Biermann et al. [73] the "normal" SuperNova explosions mainly accelerate

protons up to about 100 TeV, while more massive SuperNovae can accelerate heavier particles up to $\sim Z \cdot 10^{15}$ eV. As a consequence, the knee composition becomes heavy-dominated as the proton spectrum bends before.

- 2) *Diffusion*: the knee may reflect a change in the propagation of cosmic rays from their sources to the solar system. Analysis of the B/C ratio shows that the "escape time" of CRs from our Galaxy scales with energy according to $\tau_{\text{esc}} \propto E^{-\delta}$ with $\delta \approx 0.6$. A simple extrapolation of τ_{esc} to higher energies breaks down at $E \approx 3 \cdot 10^{15}$ eV, because here $c\tau_{\text{esc}} \sim 300$ pc which is the thickness of the Galactic disk [74]. The value corresponds to just one crossing of the disk and would give rise to significant anisotropies with respect to the Galactic plane when approaching this value. A compilation of the anisotropy measurements is given in [75]. While the amplitude and phase of anisotropy data below $\simeq 2 \cdot 10^{14}$ eV are consistent and statistically accurate [76], the experimental results at higher energies are not compatible with expectations. This could mean that the diffusion model cannot be simply extrapolated to these energies [77]. Similarly to acceleration at SNR shocks, the process of Galactic confinement is closely related to magnetic field confinement, i.e. in addition to anisotropies one again expects $E_{\text{max}} \propto Z$.
- 3) *Hadronic interactions*: in this case the idea is that the interaction of primary particles inside (or outside) the atmosphere can transfer energy to a component not observed in the EAS experiments, through a new interaction channel [79, 80, 81]. This leads to an underestimation of the reconstructed primary energy which mimics a break in the spectrum. Differently from the astrophysical interpretations 1) and 2) of the knee, one would now expect the knee energy of different primary particles being displaced following their mass number A rather than their charge Z , since the nuclear reaction mechanisms are governed by the energy per nucleon E/A of the incident particle.
- 4) *Interaction with background particles inside the Galaxy*: in this class of models the origin of the knee is related to the interaction of cosmic rays with background photons or neutrinos. Recently, Wigmans [78] suggested that inverse beta decay of protons with massive relic neutrinos, $p + \bar{\nu}_e \rightarrow n + e^+$, could deplete them. Simple kinematics shows that this channel is open for $E_p > 1.7 \cdot 10^{15} \text{ eV} / m_\nu (\text{eV})$. Thus, the knee energy $\simeq 3$ PeV would correspond to an electron neutrino mass of $\sim 0.5 \text{ eV}/c^2$, a value at the present time not excluded by any other observation or experiment. However, "eating" sufficiently large amounts of protons by such a process requires extraordinarily high local densities of relic neutrinos.

A picture related to interpretations 1) and 2) has been proposed by Erlykin and Wolfendale[56]. They consider the knee as a superposition of a weakly energy dependent galactic modulation with additional prominent structures in the flux spectrum caused by a single near by object. This so-called "single source model" assumes that a shock wave of a recent supernova which exploded some 10,000 years ago at a distance of a few hundred parsecs currently propagates, or has recently propagated, through the solar system causing distinct peaks of element groups in the energy spectrum. However, there is some controversy whether or not the statistics of presently existing data gives support to the model.

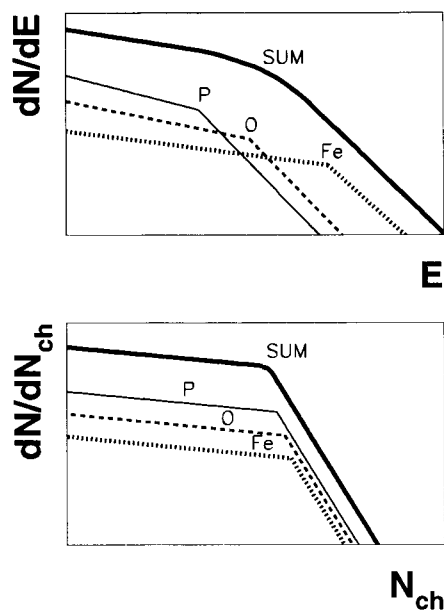


Figure 25. The sharpness of the knee for an energy (upper plot) and a size (lower plot) spectrum if a knee at the same rigidity ($= pc/Ze$) is assumed for each element.

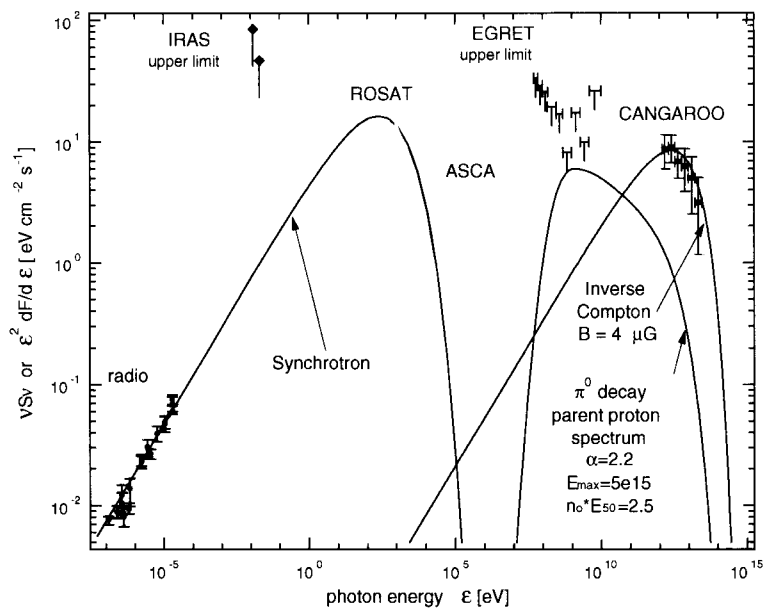


Figure 26. Multi-band spectrum of energy fluxes from SN1006 measured by different experiments. Solid lines are model fits.

Besides the position of the knee, the sharpness of the slope change is an important tool for understanding its origin. This fact can be understood from Fig.25 (adapted from [82]). The upper panel shows spectra of p, O and Fe as a function of energy. For each element a knee at the same rigidity ($= pc/Ze$) is assumed. In the lower plot the spectra for O and Fe are shifted to the right of the proton curve since showers induced by heavy nuclei are sampled in a later stage with respect to the proton ones of the same energy. Hence, the proton primaries dominate the size spectra, as compared to the energy spectrum, because the heavier nuclei have smaller electron sizes at the observational level. The resulting sum spectrum resembles more the proton size spectrum with its sharp knee.

As already discussed in sections 4.2 and 4.4, a composition insensitive method to estimate the primary energy is crucial in order to reconstruct an accurate energy spectrum. That is, if the composition changes across the knee, then the relationship between the measured electron size and inferred energy will also vary. Without an independent technique of assessing the composition, the energy spectrum can be subject to unknown systematic shifts.

As a consequence, the knowledge of the shape of the spectrum as well as of the energy spectra of different element groups across the knee region is of fundamental importance for discriminating among various possibilities. At present, beyond the knee little is known about CRs other than their all-particle energy spectrum since the indirect methods of detection suffer a number of serious difficulties in the interpretation of the data and require detailed modelling of the air shower development.

If protons are accelerated to PeV energies some of them should interact with the matter surrounding the source producing π^0 which decay into high-energy γ -rays in the TeV range. A direct evidence that the nucleonic component of CRs is indeed produced in SNRs could be obtained by the observation of γ -rays.

In the last decade there has been a lot of progress in TeV gamma-ray astronomy [83, 84], and indeed various SNRs, like RX J1713.7-3946, RX J0852-4622, Cas-A, were found to be sources of TeV γ -rays. However, considering also the measurements at lower frequency bands, in all cases the TeV γ -ray fluxes can be consistently explained with a "self-synchrotron-inverse-Compton" model, i.e., with an electron acceleration without any contribution from pion decays (Fig.26) [85]. No positive evidence for hadroproduction of TeV γ -rays has been found yet.

Recently Berezhko et al. [86] suggested a theoretical picture of a more efficient proton acceleration inside the sources which could explain the measured spectra also with γ -ray hadroproduction and a smaller contribution from inverse Compton process. Measurements of this kind provide interesting aspects in understanding the source of charged cosmic rays.

Although the great progresses in the cosmic ray research with the last generation of EAS experiment there is no unambiguous experimental results to select the best model. In fact, fundamental questions are still open:

- At which energy SNRs is the knee position?
- Is the shape of the knee sharp or smooth?
- What is the composition in the knee region? Does it change with energy?

- What is the energy spectrum of single masses? Do all primary masses show a knee feature?
- Where is the knee of the light nuclei?
- What is the dominant source for cosmic rays with energies below the knee?
- What is the origin of cosmic rays beyond the knee?
- Are the hadronic interactions at knee energies well understood?

Among different primary particles, the precise knowledge of the proton spectrum is the key for understanding the particle acceleration mechanisms, providing the major constraints on the model parameters.

6. Outlook for the Future: the Top-Game

One of the most important questions to be solved concerns the position of the proton knee. The existing experimental data are in substantial disagreement: the proton spectrum measured by the TIBET-AS γ experiment exhibit a knee-like structure around 200 TeV, the KASCADE data suggests a steepening at a few PeV, the CASA-MIA analysis show evidence of a steepening of the lighter component around 500 TeV. Direct measurements carried-out by RUNJOB and JACEE do not exhibit any spectral break up to about 800 TeV.

The knowledge of the primary proton spectrum is fundamental for the understanding of the cosmic ray acceleration mechanisms and of the propagation processes in the Galaxy. Moreover, the proton component is mainly responsible for the uncorrelated particle production in the atmosphere: any uncertainty on its spectrum reflects on the secondary particle fluxes (π and K) and thus, for example, on calculations of atmospheric muons and neutrinos.

Accordingly, a careful measurement of the proton spectrum in the energy region from 1 TeV to 100 PeV is one of the main tasks of future cosmic ray experiments.

Another important open question is the sharpness of the knee region. Data from TIBET-AS γ and CASA-MIA suggest a smooth change of slope, at variance with the results from other experiments showing a sharp knee. The actual form of the knee contains important information on its origin.

This complex situation is mainly due to the following reasons:

- All the EAS experiments (except the ones located at Chacaltaya and Tibet) sample showers at altitudes lower than 3000 m a.s.l.. Hence, they analyze showers with very large fluctuations in all the observables.
- The information about the characteristics of the primary particle (mass and energy) are diluted in an aged shower and are difficult to disentangle.

In addition, up to now, EAS data never has been calibrated with the direct measurements.

A way to reduce these problems is to perform multi-component EAS experiments at very high altitude (> 4000 m a.s.l.). In this case:

- the reduced attenuation in the atmospheric overburden allows to observe EAS with lower primary energy (\sim TeV), thus approaching the direct measurements;
- the maximum longitudinal development for showers with the knee energies is closer to observation level, so size fluctuations are reduced;
- the average shower size is almost the same for both proton and iron primaries, and therefore is an energy estimator independent of composition;
- the energy flow in the core region of EAS is less attenuated and easier to observe. As an example, at 4300 m a.s.l. for showers with the knee energies the energy flow of the electromagnetic component within 1 m from the core is 30-40 times higher than that at sea level [87].

The need to measure showers induced by cosmic rays with energies as low as 1 TeV imposes the construction of an unconventional air-shower array at high altitude. In fact, at these energies the shower particle content is too small to reconstruct the EAS observables with a typical array made of several detectors spread over a large area sampling only about 1% of the shower size.

Only the exploitation of a full coverage approach can provide the required high granularity sampling of particle showers. An experiment which can meet these requirements is the ARGO-YBJ apparatus, located at the YangBaJing (YBJ) Cosmic Ray Laboratory (Tibet, 4300 m a.s.l.).

6.1. The ARGO-YBJ Experiment

The ARGO-YBJ apparatus consists of a full coverage array of dimension $\sim 74 \times 78$ m² realized with a single layer of Resistive Plate Counters (RPCs), 280×125 cm² each. The area surrounding the central detector core, up to $\sim 100 \times 100$ m², is partially ($\sim 50\%$) instrumented with RPCs. This outer ring improves the apparatus performance, enlarging the fiducial area for the detection of showers with the core outside the full coverage carpet. A lead converter 0.5 cm thick will cover uniformly the RPCs plane. In this way the number of charged particles is increased by conversion of shower photons, thus lowering the energy threshold and reducing the particle time fluctuations on the shower front. The RPC signals are picked up by means of strips 6.7 cm wide and 62 cm long. The strips (124800 in total in the carpet) are the basic element which defines the space pattern of the shower. The fast-OR signals of 8 strips are used for time measurements and trigger purposes. These OR-ed strips define a logic PAD of 56×62 cm² (15600 in total in the carpet), which is the basic element providing the time pattern of the shower. The basic detection unit will be the Cluster, a set of 12 contiguous RPCs (see Fig.27). For a more detailed description of the experiment see [88].

This experiment will image with high efficiency and sensitivity atmospheric showers initiated by primaries of energies ≥ 200 GeV, allowing to bridge the GeV and TeV energy regions and to produce data on a wide range of fundamental issues in cosmic ray physics and γ -ray astronomy.

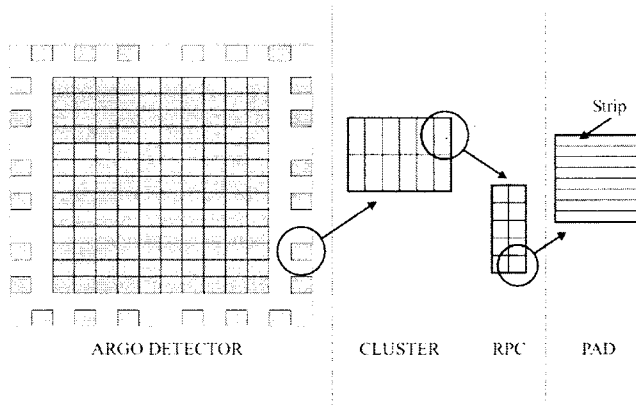


Figure 27. Layout of the ARGO-YBJ array showing the definition of Cluster, RPC, PAD, Strip.

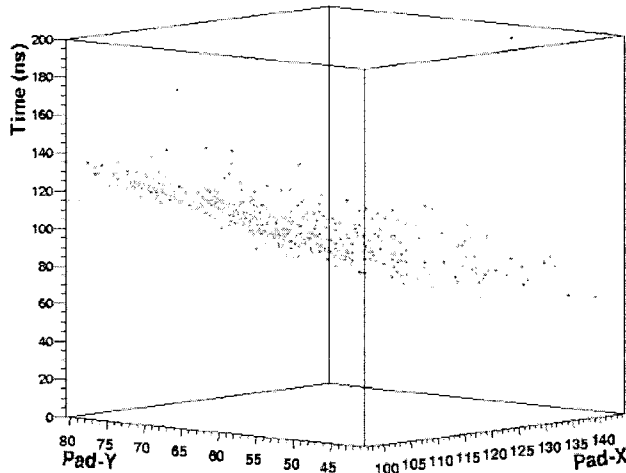


Figure 28. Picture of an air shower event sampled by the ARGO-YBJ detector.

An example of the high-granularity sampling capability of the ARGO-YBJ carpet is shown in Fig.28, where the picture of an air shower event recorded by the pad system is displayed. As can be seen, the shower profile is sampled with an unprecedented accuracy.

Both single pad rate measurements ($\sim 400 \text{ Hz}$) and expected event rates enables the experiment to run with a relatively low multiplicity (≥ 50 fired pads) triggers on the entire carpet. MonteCarlo simulations show that a Crab-like γ -ray source spectrum can be explored with threshold $\sim 200 \text{ GeV}$ and median energy $\sim 500 \text{ GeV}$, by selecting the events with a reconstructed shower core position inside the detector area. With such a multiplicity threshold ARGO-YBJ can achieve a pointing accuracy better than 1° and a sensitivity to such a point source of at least 10σ in 1 year of data taking (without considering any quality factor coming from the γ /hadron primary discrimination technique) [89].

In Fig.29 we show the average strip and pad sizes (N_s and N_{pad}) as a function of the primary energy for proton-induced showers. For comparison, the total shower size N_{ch} and

the so-called "truncated size" N_{ch}^{tr} , i.e., the size sampled by the ARGO-YBJ carpet, are also plotted. In the calculations only quasi-vertical ($\theta < 15^\circ$) showers with reconstructed core inside a small fiducial area (260 m^2 around the center of the carpet) have been used. An average strip efficiency of 95% and an average strip multiplicity $m = 1.2$ have been taken into account.

As can be seen from the figure, $\log(N_s)$ is a linear function of $\log(E)$ up to about 100 TeV and "saturates" above 1000 TeV. Accordingly, the digital response of the detector can be used to study the primary spectrum up to energies of a few hundreds TeV. In order to extend the dynamic range up to PeV energies, a charge read-out has been implemented by instrumenting each RPC also with two large size pads of dimension $140 \times 125 \text{ cm}^2$ each [90, 91].

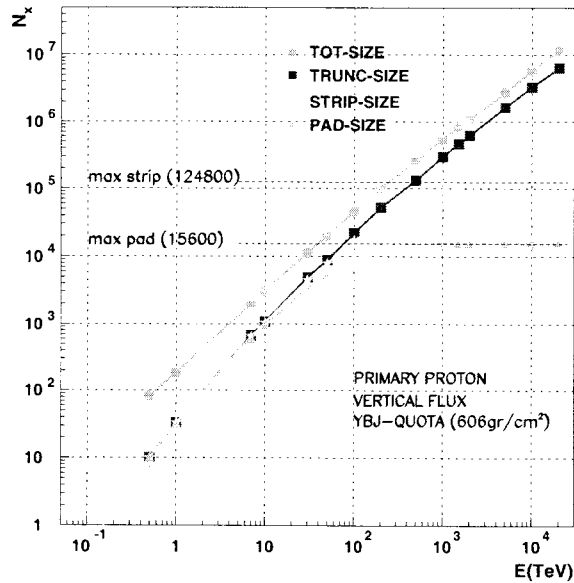


Figure 29. Average strip and pad sizes compared to the total and truncated sizes for proton-induced air showers.

6.2. The Shower Size Distribution

The study of shower size distributions at the Yangbajing atmospheric depth has been performed by means of the CORSIKA/QGSJet code in the energy range 500 GeV – 20 PeV. The probability that a cosmic ray nucleus with mass A and energy E will produce a shower with a size in the range from y to $y + \Delta y$ at the YBJ observation level is gaussian in the logarithm of the charged particle size y ($y = \log(N_{ch})$)

$$P_A(y, E) \cdot \Delta y = \frac{1}{\sqrt{2\pi} \cdot \sigma_y(A, E)} \cdot e^{-\frac{1}{2} \left[\frac{y(A, E) - \bar{y}(A, E)}{\sigma_y(A, E)} \right]^2} \cdot \Delta y \quad (6)$$

The optimal values of the different parameters are given in [92]. In Fig.30 some shower

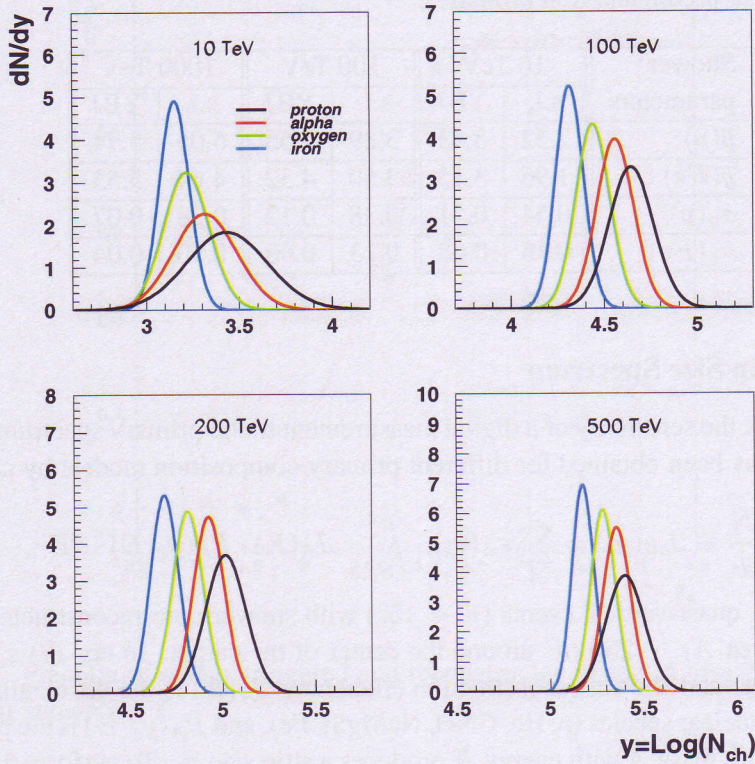


Figure 30. Shower size distributions for different nuclei at fixed primary energies.

size distributions are compared for different nuclei at fixed primary energies. From these plots it results:

- at a given energy the shower size fluctuations and the mean shower size decrease as the primary mass increases;
- increasing the primary energy the mean shower size converges to the same value for all masses.

In Tab. 1 we compare the shower gaussian parameters at sea level and at YBJ atmospheric depth. As expected, at high altitude, the size difference $\Delta y = \bar{y}(p) - \bar{y}(Fe)$ and the fluctuations σ_y due to the cascade processes are significantly smaller. In fact, we have

$$\Delta y(YBJ) \approx \frac{1}{2} \cdot \Delta y(s.l.)$$

$$\sigma_y^p(YBJ) \approx \frac{1}{3} \cdot \sigma_y^p(s.l.)$$

$$\sigma_y^{Fe}(YBJ) \approx \frac{1}{2} \cdot \sigma_y^{Fe}(s.l.)$$

Table 1. Shower parameters calculated at sea level (s.l.) and at YBJ atmospheric depth (4300 m a.s.l.) for proton and iron primaries.

Shower parameters	10 TeV		100 TeV		1000 TeV	
	s.l.	YBJ	s.l.	YBJ	s.l.	YBJ
$\bar{y}(p)$	2.52	3.43	3.89	4.65	5.05	5.74
$\bar{y}(Fe)$	1.96	3.15	3.50	4.32	4.64	5.53
$\sigma_y(p)$	0.54	0.21	0.38	0.12	0.28	0.07
$\sigma_y(Fe)$	0.18	0.08	0.13	0.08	0.10	0.04

6.3. The Strip Size Spectrum

In order to check the sensitivity of a digital measurement to the primary spectrum, the strip size spectrum has been obtained for different primary composition models by calculating the flux

$$\frac{dN}{dy_s} \equiv J_{all}(y_s) = \sum_A \varepsilon_A(y_s) \cdot \int_{E_{min}}^{\infty} J_A(E) \cdot P_A(y_s, E) \cdot dE \quad (7)$$

and by selecting quasi-vertical events ($\theta < 15^\circ$) with shower core reconstructed inside a small fiducial area $A_f \sim 260 \text{ m}^2$ around the center of the carpet. In eq. (7) $\varepsilon_A(y_s)$ represents the trigger and shower reconstruction efficiency, $J_A(E)$ is the differential flux for each simulated nuclear species (p, He, CNO, NeMgSi, Fe), and $P_A(y_s, E)$ is the probability that a nucleus with mass A with energy E produces a strip size y_s . To perform the calculations the following primary composition models have been used: RUNJOB [9], JACEE [6], TIBET-AS γ [64] and the model proposed by Horandel to reproduce the KASCADE data [93].

The reconstruction procedure is given in [94, 99, 96]. The efficiency $\varepsilon_A(y_s)$ is shown in Fig.31. The proton-induced showers are reconstructed with efficiency 1 when $y_s \geq 3.6$ (i.e., $E \geq 30 \text{ TeV}$), while the iron-induced ones when $y_s \geq 3.3$ (i.e., $E \geq 50 \text{ TeV}$).

The probabilities $P_A(y_s, E)$ for the selected events can be described by the gaussian form (6) written for the logarithm of the strip size with the parameters given in [92].

The integration of eq. (7) has been performed numerically and the results are shown in Fig.32 where, for each composition model investigated, the function

$$F_{all}(y_s) = J_{all}(y_s) \cdot 10^{1.5 \cdot y_s} \cdot \Gamma \cdot \Delta y_s \quad (8)$$

is plotted. This equation provides in a simple way the counting rate of collected events, $C_s(y_s)$, integrated in the bin $\Delta y_s = 0.1$ for an exposure $\Gamma = 10^8 \text{ m}^2 \cdot s \cdot sr$,

$$C_s(y_s) = \frac{F_{all}(y_s)}{10^{1.5 \cdot y_s}} \quad (9)$$

corresponding to about one month of data taking for quasi-vertical showers with the core position reconstructed inside the fiducial area A_f . The slope of the strip size spectrum ($J_{all}(N_s) \propto N_s^{-\alpha_s}$) in the range $y_{s1} \div y_{s2}$ is given by

$$\alpha_s = 2.5 - \frac{\text{Log}[F_{all}(y_{s2})/F_{all}(y_{s1})]}{y_{s2} - y_{s1}} \quad (10)$$

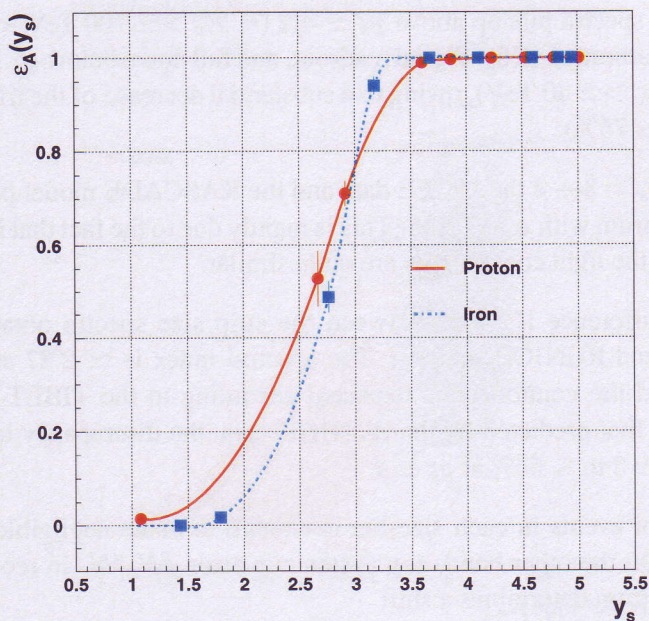


Figure 31. Fraction of events triggered and reconstructed inside A_f for proton- and iron-induced air showers.

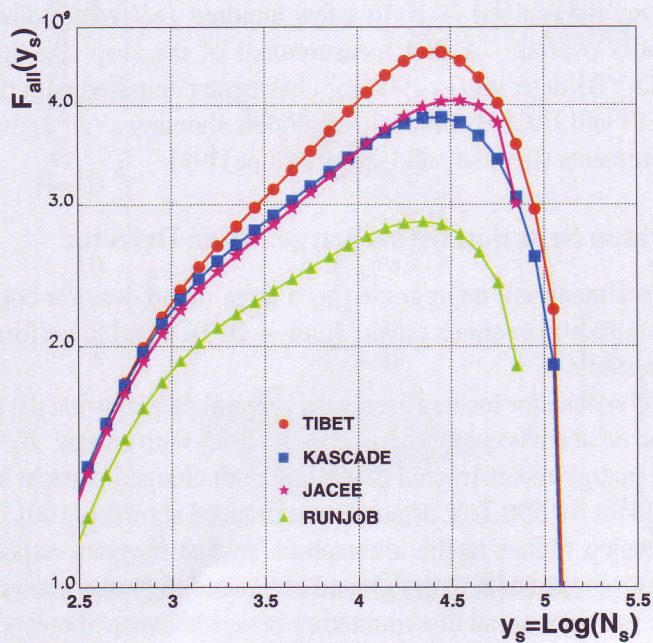


Figure 32. The strip size spectrum for the primary composition models investigated.

From Fig.32 we can draw the following conclusions:

1. The strip size spectra pile up above $y_s \simeq 4.2$ ($\langle E_p \rangle \simeq 100$ TeV, $\langle E_{Fe} \rangle \simeq 320$ TeV), due to saturation of the digital read-out, and fall down below $y_s \simeq 3$ ($\langle E_p \rangle \simeq 10$ TeV, $\langle E_{Fe} \rangle \simeq 40$ TeV), owing to a substantial decrease of the trigger efficiency ($\varepsilon_A(y_s = 3) \simeq 75\%$).
2. In the range $y_s = 3 \div 4$ the JACEE data and the KASCADE model predict the same strip size spectrum with $\alpha_s \simeq 2.35$. This is mainly due to the fact that in these models the spectra of the light components are quite similar.
3. The largest difference is found between the strip size spectra obtained using the TIBET-AS γ and RUNJOB models. The spectral index is $\simeq 2.27$ and $\simeq 2.37$, respectively, and the counting rate expected according to the TIBET-AS γ spectrum is higher than that predicted by the RUNJOB data, the discrepancy increasing from $\sim 30\%$ at $y_s \simeq 3$ to $\sim 55\%$ at $y_s \simeq 4$.
4. The number of events in each size bin is enough to make negligible the statistical uncertainty. On the other hand, any systematic error $\delta N_s/N_s$ in reconstructing the strip size spectrum determines a shift

$$\Delta F_{all}/F_{all} = (\delta N_s/N_s + 1)^{\alpha_s - 1} - 1. \quad (11)$$

Thus, a control of the detector performance at a level better than 10% is required in order to reduce any systematic effect below 15%.

We conclude that the digital read-out of ARGO-YBJ should allow one to scan, in a simple way, the energy range from ~ 10 to a few hundred TeV where direct and indirect measurements partially overlap. A first measurement of the strip size spectrum with a portion of the ARGO-YBJ detector (~ 1900 m²) has been compared with the expectations according to RUNJOB and JACEE composition models showing a fair agreement with the data of direct measurements (intensity and spectra slope) [98].

6.4. Primary Proton Selection with a Large Muon Detector

The ARGO-YBJ experiment will be upgraded by a large muon detector both to extend the sensitivity to γ -ray sources to energies greater than ~ 20 TeV and to perform a cosmic ray primary composition study.

A ~ 2500 m² muon detector located around the central carpet inside the building which hosts the detector has been envisaged to detect EAS muons with energy $E_\mu \geq 1$ GeV [97]. The shower primary energy reconstructed exploiting both charged particle and muon sizes is better than 20% (14%) for 500 TeV proton (iron) induced showers [100].

Iron showers develop higher in the atmosphere so that they are expected to have a slightly broader lateral distribution on the ground compared to proton showers of the same energy. This feature provides some discriminatory power between showers from different primaries but with the same ground-level size. In fact, if a proton and an iron shower have the same size then the proton one will have on average higher particle densities near its core.

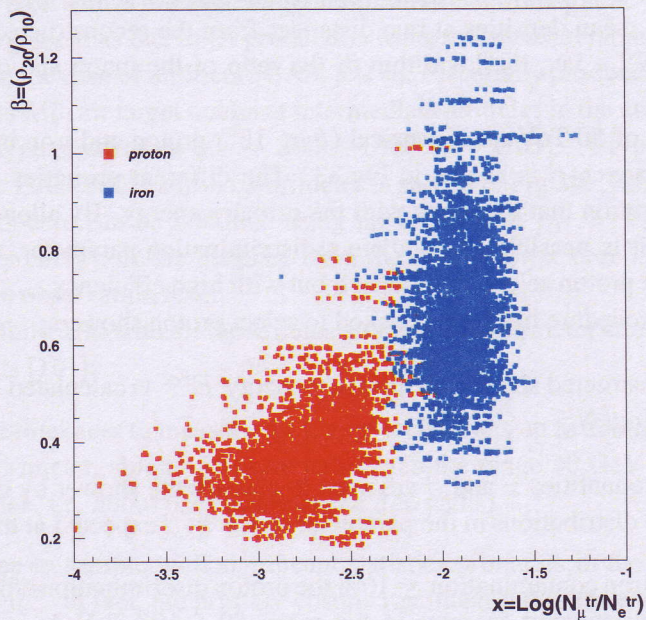


Figure 33. Distribution of proton and iron induced showers in the parameter space $x-\beta$.

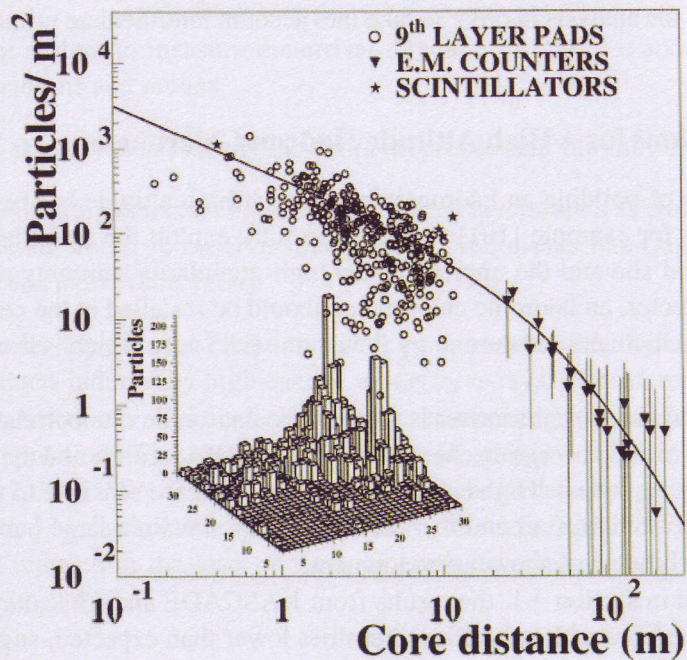


Figure 34. A multicore EAS sampled by the EAS-TOP calorimeter: the lateral distribution and the core region are shown.

As a consequence, in order to discriminate between proton and iron events the showers can be classified in terms of the two following parameters: (1) $\beta = \rho_{20}/\rho_{10}$, i.e., the ratio of charged particles mean densities at two distances from the reconstructed core position; (2) $x = \log(N_{\mu}^{tr}/N_{ch}^{tr})$, i.e., the logarithm of the ratio of the muon and charged particle truncated sizes.

The distribution of 50 TeV quasi-vertical ($\theta < 15^\circ$) proton and iron induced showers in the parameter space $x-\beta$ is shown in Fig.33. The different primaries are gathered in clusters with a separation that increases with the primary energy. By allowing for a small iron contamination it is possible to calculate a discrimination parameter, function of the energy, such that the proton selection is carried out with high efficiency.

The following procedure has been checked to select proton showers:

1. for each reconstructed shower the primary energy E^{rec} is calculated via the formula $\log(E^{rec}) \sim \log(N_{ch}^{tr} + \xi \cdot N_{\mu}^{tr})$;
2. the measured quantities x and β are used to classify the shower by comparing their value with the distributions in the parameter space $x-\beta$ expected at the energy E^{rec} .

By requiring an iron contamination $\leq 10\%$ the proton discrimination efficiency is better than 95% for the investigated energies in the range $50 - 10^4$ TeV. In order to improve the energy resolution, the primary energy of "proton-like" events could be reevaluated by means of a relation specialized to proton-induced showers. The results are encouraging and show that the shower density profile and the muon content are a powerful mass and energy identifiers and could enable the selection of a "good" sample of proton induced events. An improvement of the analysis in order to take into account intermediate primary mass groups is in progress.

6.5. Suggestions for a High Altitude Hadron Calorimeter

The opportunity of building an hadron calorimeter at high altitude has been discussed in some papers, as for example [101]. In order to fully exploit the potential of a high altitude experimental site and the unprecedented high-granularity sampling capability of the ARGO-YBJ detector, an hadronic calorimeter should be installed in the central part of the carpet. In fact, at high altitude the energy flow in the EAS core region is less attenuated and easier to observe.

The aim of an hadron calorimeter is to study the hadron flux, uncorrelated and in EAS, the energy content and absorption characteristics of the EAS cores, and the peculiar events (such as the large p_T ones). High energy air shower cores are sensitive to the composition of the primary cosmic rays around the knee since they contain a large part of the primary energy in the early stage of shower development.

As discussed in section 3.1, the results from KASCADE and Chacaltaya experiments, which observe hadrons and γ -families intensities lower than expected, suggest that, in the energy range $10^{15} - 10^{16}$ eV, a larger dissipative mechanism occurs in hadron interactions compared to current models predictions. Consequently, a careful measurement of the hadronic component is crucial to study the main features of high energy hadronic interactions in the still unknown very forward region.

This kinematical region can be studied also by means of the so-called "multicore events", i.e., events with a multiple structure in their electromagnetic component near the core. Interpreting them as due to jet production leads to a measurement of the cross section $(d\sigma/dp_T)_{pN}^{jet}$. In the case of multicore EAS, jets are essentially produced by the leading particle interactions with air target nuclei at intermediate altitudes in the atmosphere ($\sim 6 - 12$ km a.s.l.), for typical energies $\sqrt{s} \sim 300 - 1000$ GeV [103]. A typical multicore event observed by the EAS-TOP hadron calorimeter is shown in Fig.34. The transverse momentum for each subcore can be obtained using the expression $p_T = \frac{E_s R}{h}$, where E_s is the subcore primary energy, R the distance from the main shower core and h the production height above the observation level.

In order to fully deal with all these items an hadron calorimeter should meet the following requirements [101]:

- (a) Adequate thickness to measure the energy of hadrons up to about 100 TeV (the EAS-TOP calorimeter, able to measure hadrons in the range 30 GeV - 100 TeV, was 818 g/cm² thick, i.e. about 6.2 nuclear mean free paths).
- (b) Large area to sample with significant statistics primaries in the knee region, i.e. at least 100 m². In fact, the primary cosmic ray integral flux for energies above 10 PeV is about 1 particle/(m² · year).
- (c) A high granularity sampling on the top to observe the multicore structure of the shower electromagnetic component. The RPC counters operating in the ARGO-YBJ carpet greatly meet this requirement.
- (d) A tracking system to measure the arrival direction of particles and to discriminate between hadrons and muons.
- (e) A time-of-flight system to study the temporal profile near the shower core.
- (f) Fine grain tracking detectors between its different layers, such as emulsion chambers or scintillating fibers, to observe strange and exotic events like Centauros, chions, binocular and halo events [104].

At high altitude, however, the electromagnetic component in the core is mostly made by the cascade products induced by high energy π^0 -decay γ -rays. Therefore, this component well reflects the behaviour of the whole hadronic component, keeping the sensitivity to the primary composition. The observation of the high energy e.m. component has been exploited by the TIBET-AS γ experiment by means of a burst detector, a single layer plastic scintillator covered by lead plates, which measures the size of the local showers (the so-called "bursts") induced in the lead by the high energy electromagnetic component [87, 102].

7. Conclusions

The first indication for the so-called knee in the primary cosmic ray energy spectrum was obtained more than 40 years ago. In spite of large progresses in building multi-component

EAS experiments and in the analysis techniques, the origin of this phenomenon remains still unsolved. There are significant discrepancies among the different measurements concerning the position and the sharpness of the knee and the chemical composition of the primary cosmic radiation. The main reason is that there are no direct measurements in the knee region, so that all data comes from air shower arrays. The consequence is an intrinsic ambiguity on the interpretation of cosmic ray data, since it is impossible to deduce both the composition and the dynamics of particle interactions in the fragmentation region, basing on a single measurement.

A way to bring towards solution the knee problem is to perform a multi-component EAS experiment at very high altitude (> 4000 m a.s.l.). The ARGO-YBJ experiment, located at the YangBaJing Cosmic Ray Laboratory (Tibet, 4300 m a.s.l.), can provide a unique opportunity to study the cosmic radiation in the knee region. The low energy threshold (~ 200 GeV) and the high granularity sampling allow the continuous monitoring of the γ -ray emission from SNRs, the most probable sources of cosmic rays. In addition, as discussed in section 6.3, the digital read-out of ARGO-YBJ should allow to scan, in a simple way, the energy range from ~ 10 to a few hundred TeV, where direct and indirect measurements partially overlap, discriminating between different models for the primary cosmic ray composition. This range can be extended towards higher energies by means of the RPC analog read-out. By equipping the experiment with a large muon detector, an efficient selection of a primary proton beam could be achieved.

Finally, the opportunity of operating an hadron calorimeter at high altitude has been presented. The detection of the energy flow in the EAS core region is expected to clarify unknown features of the hadronic interactions in the very forward region, reducing the uncertainties of the MC simulations used to interpret the cosmic ray data.

Acknowledgements

We would like to thank B. D’Ettorre Piazzoli and T. Di Girolamo for comments and clarifying discussions about the subject of this paper.

References

- [1] Kulikov, G. V.; Khristiansen, G. B. *Sov. Phys. JETP* 1959, 8, 41.
- [2] Peters, B. J. *Geophys. Research* 1959, 64, 155.
- [3] Lagage, P. O.; Cesarsky, C. J. *Astron. Astrophys.* 1983, 125, 249.
- [4] Watson, A. *25th ICRC Rapporteur Talk Proc.*, Durban, RS, 1997; 21.
- [5] Shibata, T. *Nucl. Phys. Proc. Suppl.* 1999, 75A, 22.
- [6] Asakimori, K. et al. *ApJ* 1998, 502, 278.
- [7] Cherry, M. *26th ICRC Proc.*, Salt Lake City, US, 1999; Vol. 3, 187-190.

- [8] Ivanenko, I. P. et al. *23th ICRC Proc.*, Calgary, CD, 1993; Vol. 2, 17.
- [9] Apanasenko, A. V. et al. *Astrop. Phys.* 2001, 16, 13.
- [10] Apanasenko, A. V. et al. *26th ICRC Proc.*, Salt Lake City, US, 1999; Vol. 3, 163.
- [11] Furukawa, M. et al. *28th ICRC Proc.*, Tsukuba, JP, 2003; Vol. 4, 1837.
- [12] Furukawa, M. et al. *28th ICRC Proc.*, Tsukuba, JP, 2003; Vol. 4, 1885.
- [13] Aglietta, M. et al. *Nucl. Instr. Meth.* 1993, A336, 310.
- [14] Kamata, K.; Nishimura J. *Progr. Theoret. Phys. Suppl.* 1958, 6, 93.
- [15] Greisen, K. *Progress in Cosmic Ray Physics*, North Holland, NL, 1956; vol. 3.
- [16] D'Ettorre Piazzoli, B.; Di Sciascio G. *Astrop. Phys.* 1994, 2, 199-214.
- [17] Greisen, K. *Ann. Rev. Nucl. Sci.* 1960, 10, 63.
- [18] Navarra, G. et al. *Nucl. Phys. Proc. Suppl.*, 1998, B60, 105.
- [19] Antoni, T. et al. *Astrop. Phys.* 2001, 14, 245.
- [20] Navarra, G. et al. *27th ICRC Proc.*, Hamburg, GE, 2001; Vol. 1, 120.
- [21] Haungs, A. et al. *Rep. Prog. Phys.* 2003, 66, 1145.
- [22] Costa, C. G. S. *Phys. Rev.* 1998, D57, 4361.
- [23] Jones, L. W. *CERN Courier* 2001, 27, 1785.
- [24] Heck, D. et al. *27th ICRC Proc.*, Hamburg, GE, 2001; Vol. 1, 233.
- [25] Amos, N. A. et al. *Phys. Rev. Lett.* 1992, 68, 2433.
- [26] Abe, F. et al. *Phys. Rev.* 1992, D50, 5550.
- [27] Avila, C. et al. *Phys. Lett.* 1999, B445, 419.
- [28] Antoni, T. et al. *J. Phys.* 2001, 27, 1785.
- [29] Heck, D. et al. *Report FZKA 6019*, Forschungszentrum Karlsruhe, GE, 1998.
- [30] Kalmykov, N. N.; Ostapchenko, S.S. *Yad. Fiz.* 1993, 56, 105.
- [31] Ave, M. et al. *27th ICRC Proc.*, Hamburg, GE, 2001; Vol. 1, 385.
- [32] Brun, R. et al., *Report CERN* 1994, W5013.
- [33] Knapp, J. et al. *Astrop. Phys.* 2003, 19, 77.
- [34] Kampert, K.-H. et al. *27th ICRC Invited Rapporteur Highlight papers*, Hamburg, GE, 2001; 240.

-
- [35] Aguirre, C. et al. *Phys. Rev.* 2000, D62, 032003.
- [36] Kawasumi, N. et al. *Phys. Rev.* 1996, D53, 3534.
- [37] Lipari, P. *Nucl. Phys. Proc. Suppl.* 2003, 122, 133-148.
- [38] Castellina, A. *Nucl. Phys. Proc. Suppl.*, 2001, B97, 35.
- [39] Sommers, P. *27th ICRC Invited Rapporteur Highlight papers*, Hamburg, GE, 2001; 170.
- [40] Horandel, J.R. *Astrop. Phys.* 2003, 19, 193.
- [41] Aglietta, M. et al. *Astrop. Phys.* 1999, 10, 1.
- [42] Aglietta, M. et al. *Nucl. Phys. Proc. Suppl.* 2000; B85, 318.
- [43] Aglietta, M. et al. *Nucl. Phys. Proc. Suppl.* 1999; A75, 251.
- [44] Aglietta, M. et al. *Astrop. Phys.* 2003, 19, 329-338.
- [45] Aglietta, M. et al. *26th ICRC Proc.*, Salt Lake City, US, 1999; Vol. 1, 230.
- [46] Navarra, G. et al. *27th ICRC Proc.*, Hamburg, GE, 2001; Vol. 1, 120.
- [47] Aglietta, M. et al. *preprint astro-ph/0112473*, 2001.
- [48] Aglietta, M. et al. *Astrop. Phys.* 2004, 20, 641.
- [49] Aglietta, M. et al. *preprint astro-ph/0112475*, 2001.
- [50] Bertaina, M. et al. *28th ICRC Proc.*, Tsukuba, JP, 2003; Vol. 1, 115.
- [51] Klages, H.O. et al. *Nucl. Phys. Proc. Suppl.* 1999, B52, 92.
- [52] Haungs, A. et al. *Acta Phys. Polon.*, 2004, B35, 331-339.
- [53] Haungs, A. et al. *preprint astro-ph/0508286*, 2005.
- [54] Antoni, T et al. *Nucl. Phys. Proc. Suppl.* 1999, 75A, 234.
- [55] Roth, M. et al. *28th ICRC Proc.*, Tsukuba, JP, 2003; Vol. 1, 139.
- [56] Erlykin, A. D.; Wolfendale, A. W. *J. Phys.* 1997, G23, 979.
- [57] Berezhko, E.G.; Ksenofontov, L.T. *J. Exp. Theor. Phys.* 1999, 89, 391.
- [58] Swordy, S. *24th ICRC Proc.*, Rome, IT, 1995; Vol. 2, 697.
- [59] Kampert, K.-H. et al. *preprint astro-ph/0204205*, 2002.
- [60] Borione, A. et al. *Nucl. Instrum. Methods* 1994, A346, 329.
- [61] Glasmacher, M. A. K. et al. *Astrop. Phys.* 1999, 10, 291.

- [62] Glasmacher, M. A. K. et al. *Astrop. Phys.* 1999, 12, 1.
- [63] Amenomori, M. et al. *ApJ* 1996, 461, 408.
- [64] Amenomori, M. et al. *Phys. Rev.* 2000, D62, 112002.
- [65] Amenomori, M. et al. *28th ICRC Proc.*, Tsukuba, JP, 2003; Vol. 1, 107.
- [66] Amenomori, M. et al. *Phys. Lett.* 2006, B632, 58.
- [67] Kampert, K.-H. et al., *Acta Phys. Polon.*, 2004, B35, 1799.
- [68] Fowler, J.W. et al. *Astrop. Phys.* 2001, 15, 49.
- [69] Swordy, S.P. et al. *Astrop. Phys.* 2000, 13, 137.
- [70] Horandel, J.R. *preprint astro-ph/0402356*, 2004.
- [71] Kampert, K.-H. Tihany 2000, *From $e^+ e^-$ to heavy ion collisions (ISMD 2000)*, 2001, 235-243.
- [72] Drury, L. O'C. *Contemp. Phys.* 1994, 35, 231.
- [73] Biermann, P. L. et al. *preprint astro-ph/0302201*, 2003.
- [74] Gaissler, T. K. *AIP Conf. Proc.*, 2001, 558, 27-42.
- [75] Clay, R. W. et al. *25th ICRC Proc.*, Durban, SA, 1997; Vol. 4, 185.
- [76] Aglietta, M. et al. *ApJ* 1996, 470, 501.
- [77] Hillas, A. M. *26th ICRC Proc.*, Salt Lake City, US, 1999; Vol. 4, 225.
- [78] Wigmans, R. *Astrop. Phys.* 2003, 19, 379.
- [79] Nikolsky, S. I. *Nucl. Phys. Proc. Suppl.* 1995, 39A, 228.
- [80] Kazanas, D.; Nicolaidis, A. *27th ICRC Proc.*, Hamburg, GE, 2001; Vol. 5, 1760.
- [81] Dova, M. et al. *27th ICRC Proc.*, Hamburg, GE, 2001; Vol. 5, 1780.
- [82] Knapp, J. *Nucl. Phys. B Proc. Suppl.* 1999, 75A, 89.
- [83] Ong, R. *Phys. Rep.* 1998, 305, 93.
- [84] Ong, R. *29th ICRC Proc.*, Pune, India, 2005; Vol. 10, 329.
- [85] Tanimori, T. et al. *27th ICRC Proc.*, Hamburg, GE, 2001; Vol. 6, 2465.
- [86] Berezhko, E.G. et al. *Astron. Astrop.* 2002, 395, 943.
- [87] Xu, X. W. et al. *J. Phys.*, 2003, G29, 719.
- [88] Di Sciascio G., *AIP Conf. Proc.*, 2005, 745, 663.

- [89] Vernetto, S. et al. *28th ICRC Proc.*, Tsukuba, JP, 2003; Vol. 5, 3007.
- [90] Iacovacci, M. et al. *28th ICRC Proc.*, Tsukuba, JP, 2003; Vol. 2, 757.
- [91] Creti, P. et al. *29th ICRC Proc.*, Pune, India, 2005; Vol. 8, 97.
- [92] Saggese, L. *Ph.D. Thesis*, Naples University 2003.
- [93] Horandel, J.R. et al. *27th ICRC Proc.*, Hamburg, GE, 2001; Vol. 1, 71.
- [94] Saggese L. et al. *28th ICRC Proc.*, Tsukuba, JP, 2003; Vol. 1, 263.
- [95] Di Sciascio, G.. et al. *28th ICRC Proc.*, Tsukuba, JP, 2003; Vol. 5, 3015.
- [96] Di Sciascio, G. and Rossi, E., *astro-ph/0309108* and *astro-ph/0309109*.
- [97] Di Sciascio G. et al., *AIP Conf. Proc.*, 2005, 745, 669.
- [98] Saggese, L. and Rossi E. *29th ICRC Proc.*, Pune, India, 2005; Vol. 6, 37.
- [99] Di Sciascio, G.. et al. *28th ICRC Proc.*, Tsukuba, JP, 2003; Vol. 5, 3015.
- [100] Di Sciascio G. et al., *Int. Journ. of Mod. Phys. A*, 2005, 20, 6805.
- [101] Saavedra, O.; Jones, L. W. *Nuovo Cimento* 2001, C24, 497.
- [102] Amenomori, M. et al. *Phys. Rev.* 2000, D62, 072007.
- [103] Aglietta, M. et al. *Phys. Lett.* 1999, B460, 474.
- [104] Lippman P. et al. *CERN-LHCC-97-45*, 1997, 70.